NASA-CR-192555

May, 1992

LMSC/P073417

IN-92-CR
163056
P.68

FINAL REPORT

NASA Contract NAS8-39395

Investigation of Solar Active Regions at High Resolution by Balloon Flights of the Solar Optical Universal Polarimeter

Extended Definition Phase

Performing Organization

Research and Development Division
Lockheed Missiles and Space Company, Inc.

Principal Investigator

Dr. Theodore D. Tarbell
Lockheed Palo Alto Research Laboratory
Department 91-30, Building 252
3251 Hanover St.
Palo Alto, CA 94304 phone: (415)-424-4033
Email: SPAN SOLAR::TTARBELL fax (415)-424-3994

Period of Performance

May, 1992 to May, 1993

(NASA-CR-192555) INVESTIGATION OF SOLAR ACTIVE REGIONS AT HIGH RESOLUTION BY BALLOON FLIGHTS OF THE SOLAR OPTICAL UNIVERSAL POLARIMETER, EXTENDED DEFINITION PHASE Final Report, May 1992 - May 1993 (Lockheed Missiles and Space Co.) 68 p

N93-27029

Unclas

G3/92 0163056

On November 16, 1988, the Principal Investigator, Dr. Theodore D. Tarbell, received a letter from Dr. Stanley Shawhan of NASA Headquarters stating that the proposal for "An Investigation of Solar Active Regions at High Resolution by Balloon Flights of SOUP" was accepted for a definition phase. The nominal program was to be four years long, consisting of definition phase, confirmation for flight, test flight and long duration flight. The letter stated very clearly that the Max '91 Solar Balloon Program was highly cost constrained and that the investigation would have to be carried out for the costs proposed or be descoped or cancelled. The project was to begin January 1, 1989.

The flight investigation phase of this contract was cancelled by NASA Headquarters in January, 1990, due to budgetary problems, and we were directed to devote our remaining resources to a variety of tasks. The remaining tasks, upon which Lockheed, NASA HQ and MSFC agreed, were scientific analysis and publication of data from ground-based observing with SOUP instrument components, completing the test report on low-voltage piezoelectric transducers for use in the image motion compensation system, and submission of a final report on the balloon project definition phase. This was done and the contract finally expired in April, 1992.

In January, 1992, four people from LPARL attended the Solar Research Base Enhancement Workshop (on other funds). NASA showed renewed interest in balloon flights of optical telescopes, and Tarbell and Title contributed to the RBE report chapters on ground- and balloon-based observing. The present contract was opened in May, 1992, to extend and augment these definition phase activities for another year. This contract continued technical studies of the feasability of balloon flights of the the former Spacelab instrument, the Solar Optical Universal Polarimeter, with a modern charge-coupled device (CCD) camera, to study the structure and evolution of solar active regions at high resolution. In particular, different CCD cameras were used at ground-based solar observatories with the SOUP filter, to evaluate their performance and collect high resolution images. Some of this data has been collected in coordinated observations with the Yohkoh satellite and is being analyzed scientifically.

In the spring of 1992, the SOUP tunable filter instrument was set up in our lab in Palo Alto to evaluate the SOHO MDI breadboard CCD camera. This uses a Loral (formerly Ford Aerospace) detector built specifically for MDI, a 1024 x 1024 array of 21 micron pixels. We used it to take both high resolution and full disk solar images in narrowband light at various wavelengths from 5173 to 6768 Angstroms. This detector has insignificant fringing in narrowband light, and the gain variations are removed by simple flat-fielding using defocussed images. Longitudinal magnetograms and Dopplergrams were made from the filtergrams. The images are very pretty cosmetically and have low noise and high linearity; the seeing is not very good and so the full disk images are more presentable. Since these detectors and cameras are being exhaustively calibrated and space qualified, they are good candidates for a future flight instrument.

In late April, Dick Shine and Darrel Torgerson travelled to La Palma, Canary Islands, and set up the SOUP tunable filter with the OSL brassboard CCD camera, which uses

a 1024 x 1024 18 micron detector built by TI-Japan. This camera works well both with the tunable filter and with our narrowband K-line filter (3933 Angstroms), showing vastly greater blue and near-UV sensitivity than the Loral chip. We observed from early May through early July at the Swedish Solar Tower on La Palma, in four shifts: Dick Shine, assisted by Igor Zayer of ARC (1 May to 15 May); Ken Topka, assisted by Pete Nisenson of Harvard (15 May to 1 June); Zoe Frank, assisted by Louis Strous of Utrecht (1 June to 16 June); and Ted Tarbell, assisted by Han Uitenbroek of Harvard, Jose del Toro of the Instituto Astrofisica de Canarias, and Goran Scharmer of Stockholm Observatory (16 June to 6 July). This contract only supported a small fraction of this observing run; most of the effort was supported by the OSL contract and by our collaborators.

At La Palma, our primary goal was to collect high-resolution longitudinal and transverse magnetic and H-alpha observations of active regions, simultaneous with X-ray observations of the same areas by the Yohkoh satellite. We almost always followed the Yohkoh target region and usually stayed in phase with the sunlit parts of its orbit. We obtained not only simultaneous observations of flares, but also of quiet sun, flux emergence, sunspots, pre-flare buildup, smaller transients (micro-flares, Ellerman bombs, etc.), filament eruptions, and pre- and post-flare loops at the limb. Several mornings had very good seeing, and many full day movies of the Yohkoh target region were obtained. These contain joint observations with the X-ray telescopes of just about every type of dynamic phenomenon which occurs in solar active regions, except for a giant flare. In addition, we observed during the May 12 rocket flight of the SPDE UV and X-ray instruments built by Marilyn Bruner of Lockheed. Noteworthy observations in June and July were M flares on June 8 and July 3, the last observed in excellent seeing and fully coordinated; excellent sunspot sequences on June 16 and July 2; quiet sun and an emerging flux region on June 30; buildup and shear of a large active region on June 22-25, leading to an X flare, which unfortunately occured just after La Palma and Yohkoh sunset.

On July 16-17, the instrument was moved from the Swedish Solar Observatory on La Palma to the German Vacuum Tower Telescope on the neighboring island of Tenerife. Dick Shine, Darrell Torgerson, and Dnyanesh Mathur set up the instrument for solar observing from July 19 - August 13. Although some damage to the tunable filter control electronics occurred in the transfer, the instrument was been repaired and began observing the sun on July 21. Our German collaborators are headed by Wolfgang Schmidt of the Kiepenheuer Institute of Freiburg. The observing concentrated on vector magnetic measurements and spectroscopy of sunspots, following the Yohkoh target region much of the time. A new polarimeter developed by KIS was used with our filter, a prototype candidate for the next flight instrument of this type. It should permit much more sensitive measurements of the transverse magnetic field components, whose measurement is considered crucial for estimating energy storage in an active region and forecasting flares. In addition, careful measurements of the telescope and instrumental polarization (Mueller matrices) were made, and these will be reduced in collaboration with Axel Hoffman, who runs the Potsdam vector magnetograph in formerly East Germany.

The tests in Palo Alto of the Loral and TI-Japan CCD cameras with the SOUP tunable

filter and the successful observing runs at La Palma and Tenerife, in coordination with the Yohkoh satellite, produced a very large amount of data, both scientific and calibration. An additional CCD test was the use of integrating Cohu cameras with TI sensors to observe in the K line (3933 Angstroms) and the G-band (4308 Angstroms). These cameras were provided by the Swedish Solar Observatory on La Palma. They can run at normal video rates (30 Hz) or integrate for an arbitrary number of video frames, during which time they put out a blank video signal. When used with the SSO video digitizer and frame selection system, we were able to expose to reasonable light levels with our narrowband tunable K-line filter while selecting frames based on the sharpness in the G-band granulation image. This image can also be used afterwards to measure the atmospheric distortion in the K-line images, for removal by destretching. The sensors and cameras work adequately, with reasonable efficiency (typically about 8 frames of integration was used) and cosmetic image quality. Thus we collected large amounts of high-resolution K-line imagery simultaneous with the usual tunable filter observations.

Data processing in Palo Alto has proceeded since the observing run, so that nearly all of the tunable filter data has undergone the first pass. This includes flat field, dark current, and flaw corection, and recording of movies of each wavelength on videodisk. These movies are then used for choosing which datasets to study in detail. Some more detailed work has been done with data from May 12 (region of the SPDE rocket rocket experiment), several filament eruptions of May 13 and June 15-16, and the flares of June 8 and July 3. These include the 3 July flare movies in AR 7216; sunspot, filament eruption and flare observations in AR 7194 on 14-16 June; vector magnetic sets of a sunspot and complex neutral line in AR 7186 on 7 June; and movies of remarkable H-alpha loops on the disk and above the limb in AR 7205 on 25-26 June.

Louis Strous, graduate student of Kees Zwaan of Utrecht, spent April through September at LPARL. He was reimbursed for living expenses from this contract, in return for his role in the observing run and data analysis. He has written a comprehensive set of routines for producing magnetic and intensity movies from raw data, with corrections for both atmospheric distortion and blurring. The former are removed by destretching, with careful separation of solar flows and evolution from seeing-caused distortion. The blurring is partially compensated by boosting the high spatial frequencies in each image to match the power spectrum of the best image in the series. He applied these techniques to make a movie set of a rapidly growing active region. In Utrecht, he is analyzing the flux emergence events in these movies and writing his Ph.D. thesis on this data.

We have begun working with a long-term visitor to our lab, Dr. Jose Carlos del Toro Iniesta, of the IAC in Tenerife, on more accurate calibration of longitudinal and vector magnetograms. He has radiative transfer codes for computing Stokes profiles of our absorption lines using arbitrary model atmospheres. His initial work on Stokes-V diagnostics in Fe I 6302.5 using umbral, penumbral, flux tube and quiet photospheric models was shown at the AAS meeting. He has continued studying sunspots by making empirical models for the temperature and Doppler structure of penumbrae using tunable filter line profiles of the non-magnetic line Fe I 5576.

Considerable effort has been devoted to sharing data with our other collaborators, training them in the idiosyncracies of the instrument and our software. They include H. Uitenbroek, B. Noyes, and P. Nisenson of Harvard; E. Zweibel and graduate student B. Hindman of the University of Colorado; J. Lawrence of Cal. State Northridge; H. Jones of NSO (Tucson); P. Brandt of KIS; R. Rutten of Utrecht; and S. Tsuneta and graduate students T. Shimizu and H. Hara of Tokyo.

Three research papers publishing work which was partly supported by the contract are in the Appendices. The first two were begun before this contract but completed during its tenure; since they have already appeared in *The Astrophysical Journal*, only the title and abstract are reproduced here. A poster paper was given at the December AGU meeting in San Francisco, entitled "Simultaneous Observations of Flares in the Solar Photosphere, Chromosphere, and Corona from La Palma and Yohkoh," by Tarbell et al. Three poster papers were given at the January AAS Meeting in Phoenix: "Comparison of Active Region Facular Contrast Measurements to Simple Models," by Topka and Title; "Data Compression Experiments with High Resolution Solar Images," by Shine and Majani (JPL); and "From Filtergrams to Physical Atmospheric Magnitudes: A Prospective Diagnostic," by del Toro Iniesta, Tarbell and Ruiz Cobo (IAC). Two of these are also included in appendices.

Appendix A: Abstracts from *The Astrophysical Journal*

THE ASTROPHYSICAL JOURNAL, 403:780–796, 1993 February 1
© 1993. The American Astronomical Society. All rights reserved. Printed in U.S.A.

ON THE MAGNETIC AND VELOCITY FIELD GEOMETRY OF SIMPLE SUNSPOTS

ALAN M. TITLE, ZOE A. FRANK, RICHARD A. SHINE, THEODORE D. TARBELL, AND KENNETH P. TOPKA
Lockheed Palo Alto Research Laboratory, 3251 Hanover Street, Palo Alto, CA 94304-1191
GÖRAN SCHARMER
Swedish Royal Academy of Sciences, Stockholm Observatory, S-13336 Saltsjöbaden, Sweden
AND
WOLFGANG SCHMIDT
Kiepenheuer-Institut für Sonnenphysik, Schöneckstrasse 6, D-7800 Freiburg im Breisgau, Germany
Received 1992 January 20; accepted 1992 August 6

ABSTRACT

We have observed the disk passage of relatively simple round sunspots using a narrow-band filter and a large format CCD detector and have created magnetograms, Dopplergrams, and continuum images nearly simultaneously. The spectral resolution of the filter (88,000) allows the construction of "spectra" for all points in the field of view. The changing patterns of the line-of-sight magnetic fields with position around the spots and with position of spots on the solar disk show that the mean inclination of the magnetic field increases from 45°–50° to 70°–75° across the penumbra and that there is a fluctuation about the mean of about $\pm 18°$. These inclination changes occur on the scale of the penumbral fibrils. In addition the direction changes are large enough that a substantial fraction of the magnetic field is horizontal (parallel to the solar surface) from the mid to outer penumbra. Our Doppler data show that the Evershed flow tends to occur in the regions where the magnetic field is horizontal. Taken together these observations suggest that the Evershed flow is confined to the regions of horizontal fields, which resolves the old difficulty of nonparallelism of magnetic and flow fields in a sunspot.

We show that a simple sunspot model with azimuthal variations in inclination, but no azimuthal variations of field strength, is free from azimuthal Lorentz forces. The meridional currents which arises from the inclination variations are parallel to the field lines. This suggests that a cylindrically symmetric magnetostatic sunspot model can be perturbed into one with azimuthal variations in inclination with some adjustment in the meridional force balance.

Subject headings: Sun: magnetic fields — sunspots

1. INTRODUCTION

Even a simple round isolated sunspot is very complicated structure (Schröter 1971; Gokhale & Zwaan 1972; Cram & Thomas 1981; Garcia de la Rosa 1987; Kalman 1991). There are intensity inhomogeneities in the umbra and the penumbra, nonsteady outflows in the penumbra (Evershed flows), inward motions of bright points along the bright penumbral fibrils, and various irregular wave motions in the umbra and penumbra. Given the complexity of the intensity, flow, and wave fields, it would be surprising if the magnetic field geometry were not also complex. In this paper we discuss observations of the line-of-sight magnetic and velocity field which suggest that even a simple round spot has a mutually interacting spatially complex magnetic and flow structure.

High-resolution magnetic measurements of sunspots are difficult to obtain. Most birefringent filters are not sufficiently narrow to resolve spectrally the complex profiles of Zeeman sensitive lines in sunspots. Patrol magnetographs are usually optimized for observations outside of spots. High-resolution spectra which measure all four Stokes components with high photometric precision often do not have high spatial resolution. Further, vector magnetic field measurements made with filters and spectrographs are sensitive to errors introduced by telescope polarization. Even if good data are available, the interpretation is complex because the atmosphere of a sunspot is not well understood. In particular the local inhomogeneities of the spot may require very detailed three-dimensional radiative transfer calculations to interpret spectra properly.

The above problems have long been recognized. Observers and theoreticians have generated many clever techniques to infer properties of spots. These have often used the fact that, as a spot moves across the solar disk, the projection of its vector fields on the line of sight changes progressively. In 1908, Evershed (1909) noticed that spot spectra taken with the slit oriented in an east-west direction tended to be sloped with respect to lines of constant wavelength. Center (limb) side spectral elements were blue (red) shifted. These slopes increased as the spot approached the limb; however, slopes were noticeable even for spots which passed quite close to disk center. Evershed inferred that the changing appearance of the spot spectra was due to projection onto the line of sight of nearly radial and nearly horizontal outflow in the penumbra of sunspots. Hale et al. (1918) used spectra of Zeeman triplets taken in right and left circular polarization to measure where the field was perpendicular to the line of sight, which they called the neutral line. By following numerous spots across the disk they were able to generate a mean inclination of the magnetic field as a function of radius.

Hale et al. also observed spots as they crossed the limb in linear polarization at the wavelengths of the π component of Zeeman triplets. Because the linear polarization of the π component is in the direction of the field, this technique directly measured the

THE ASTROPHYSICAL JOURNAL, 396:351–363, 1992 September 1
© 1992. The American Astronomical Society. All rights reserved. Printed in U.S.A.

PROPERTIES OF THE SMALLEST SOLAR MAGNETIC ELEMENTS. I. FACULAR CONTRAST NEAR SUN CENTER

K. P. TOPKA, T. D. TARBELL, AND A. M. TITLE
Solar and Astrophysics Laboratory, Lockheed Palo Alto Research Laboratory, Dept 9130, B 252, 3251 Hanover Street, Palo Alto, CA 94304
Received 1991 November 12; accepted 1992 March 9

ABSTRACT

We present measurements indicating that the continuum intensity of facular areas in solar active regions, outside of sunspots and pores, is less than that of the quiet Sun very near disk center. Analysis shows that the observed continuum intensity of faculae at disk center near 5000 Å is nearly 3% less than that of the quiet Sun. The intrinsic value must be even lower than this due to our finite resolution. The continuum contrast increases rapidly away from disk center, reaching +2% at 45°. The zero-crossing point, where the contrast changes sign, occurs at 20° heliocentric angle. This is contrary to many earlier observations. The photometric data were obtained using the Lockheed tunable filter instrument at the Swedish Solar Observatory, La Palma. Filtergrams of four active regions from 1988, 1989, and 1990 are presented. These were taken with a CCD camera and include continuum images of very high spatial resolution (up to 0".3), and magnetograms (up to 0".45), which have been registered to an accuracy of better than 0".1.

These results are sensitive to the size of the magnetic flux tubes comprising faculae, to their inclinations from local vertical at the $\tau(5000) = 1$ level, and to the distribution of sizes of the flux tubes. The constraint these observations place on the size of flux tubes depends upon the value of the zero-crossing point. This is important because it is independent of our resolution. Furthermore, because the contrast is changing rapidly near disk center, the zero-crossing point is well determined. Our results indicate that most of the flux tubes in solar faculae may be very small, in the range 50–100 km in diameter. The results presented here also indicate that inclination from local vertical of about 10° at the photosphere is common on the Sun. Footpoints of opposite polarity tend to tilt toward one another.

Subject headings: Sun: facule, flocculi — Sun: magnetic fields

1. INTRODUCTION

Within active regions, outside of sunspots and pores, nearly all magnetic fields in the low photosphere of the Sun are concentrated into fine structures at or below the resolution limit of observations (~1"; see Harvey 1977 for a review). Recent observations have confirmed and extended these results, showing that the smallest magnetic elements are still too small to be observed directly, and have field strengths of order ~2000–2400 G at $\tau = 1$ and ~1200–1400 G at $\tau = 0.1$, with diameters of order 100 km (0".14, see reviews by Muller 1985 and Stenflo 1989; see Zirin 1988 for a dissenting view). This has led to the concept of the small flux tube, an unresolved region of strong magnetic flux surrounded by practically field free plasma. Models have been developed for these small flux tubes in order to predict their properties (e.g., Spruit 1976; Deinzer et al. 1984a, b; Hasan 1985; Steiner, Pneuman, & Stenflo 1986; Knölker, Schüssler, & Weisshaar 1988; Grossmann-Doerth et al. 1988; Knölker & Schüssler 1988).

Faculae are bright structures seen in the photosphere that are associated with magnetic fields. They are especially visible in the continuum near the limb, but are also visible at disk center on filtergrams taken in photospheric lines. Faculae are cospatial with chromospheric plage as seen in the wings of strong chromospheric lines such as Hα and Ca II H and K. At very high resolution the faculae consists of many small continuum bright points, usually smaller than 0".5, that are also called facular points or filigree. Larger structures, including bright facular granules and dark magnetic knots, are present in the faculae as well. The small bright points can be isolated from each other or can be clumped into chains and ringlike structures also called "crinkles" (Dunn & Zirker 1973). Isolated bright points usually reside in intergranular lanes at the junction of three or more granules, and have a lifetime of about 20 minutes (Muller 1983). All of these observed phenomena, a veritable solar zoo, probably owe their existence to the small flux tube. Its properties are also important to our understanding of active region evolution, the interaction between convection and magnetic fields, and the heating of the chromosphere and corona.

Title et al. (1990) find, from comparison of very high resolution continuum images and accurately registered simultaneous magnetograms, that at the limit of their resolution (~0".35) and registration (0".1), the continuum bright points (filigree), line center bright points, and magnetic features are coincident. The relationship is not one-to-one, however; every line center bright point has an associated magnetic feature, but many magnetic features do not have associated bright points, in either continuum or line center, especially at high magnetic filling factors. Title et al. (1992, hereafter Paper I) studied the properties of magnetic areas in an active region using simultaneous continuum, line center, Dopplergram, and magnetogram movies over 2 hr long. The observations reported in Paper I are very well suited to measure accurately the continuum intensity contrast of faculae. These data consist of continuum images (near Ni I 6768 Å) of very high resolution of a region of dense plage, with simultaneous and accurately registered magnetograms. Because these data exist as movies over 2 hr long, the effects of the 5 minute oscillation on intensity measurements can be understood and removed. The results, as reported in Paper I, are a contrast of −0.7% at $\theta = 14°$ heliocentric angle ($\mu = \cos\theta = 0.970$). These results are for one image only.

Appendix B: Paper Submitted to *Journal of Geophysical Research*

Contrast of Faculae near the Disk Center and Solar Variability

J.K. Lawrence

San Fernando Observatory

Department of Physics and Astronomy

California State University, Northridge

K.P. Topka

Solar and Astrophysics Laboratory

Lockheed Palo Alto Research Laboratory

and

H.P. Jones

NASA Goddard Space Flight Center

Laboratory for Astronomy and Solar Physics

Southwest Solar Station

National Solar Observatory

Revised February 1993

Submitted to JGR 2-22-93

Author Mailing Addresses

J.K. Lawrence, San Fernando Observatory, Department of Physics and Astronomy, California State University, Northridge, Northridge, CA 91330

K.P. Topka, Solar and Astrophysics Laboratory, Lockheed Palo Alto Research Laboratory, Dept. 9130, B 252, 3251 Hanover Street, Palo Alto, CA 94304

H.P. Jones, NASA Goddard Space Flight Center, Laboratory for Astronomy and Solar Physics, Southwest Solar Station, National Solar Observatory, P.O. Box 26732, Tucson, AZ 85726

ABSTRACT

We analyse simultaneous, or near-simultaneous, co-registered, digital, photometric images of solar photospheric intensity and line-of-sight magnetic field. Images were made with the Lockheed tunable filter instrument at the Swedish Solar Observatory, La Palma, with the Video Spectra-Spectroheliograph system at the San Fernando Observatory and with the new NASA Spectromagnetograph at the National Solar Observatory at Kitt Peak.

We study the disk-center contrasts of small magnetic elements. While active region faculae are dark at disk center quiet sun network features are bright. The field element populations of these two kinds of features are quite different. Different contrast center-limb functions must be used when estimating their irradiance or luminosity contributions. The disk center contrasts of active region faculae are color dependent and indicate a depth effect related to the H^- opacity of the facular atmosphere. This result is important for calibration of monochromatic observations of faculae to bolometric irradiance fluctuations.

We emphasize the value of cooperative observations among installations whose differing strengths are complementary.

INTRODUCTION

The Solar Maximum Mission (SMM) satellite and the onboard Active Cavity Radiometer Irradiance Monitor (ACRIM) established that the sun is a variable star. Dips in the bolometric irradiance of up to 0.3% matched the rotation of large sunspot groups across the solar disk [Willson, et al., 1981]. However, the fluctuations could not be attributed entirely to sunspots. The fit was markedly improved by inclusion of the effect of active region (AR) faculae [Hudson, 1988; Chapman, et al., 1992].

Between 1980 and 1989, the SMM/ACRIM experiment also revealed a few tenths of a percent variation of the rotationally averaged irradiance in phase with the 11 year solar activity cycle: the sun is slightly brighter on the average when it is more active. This may arise from fluctuations of widespread solar magnetic fields not associated with active regions [Foukal, et al., 1991]. These fields are found in flux tubes in the quiet sun (QS) "network" between the supergranular convection cells over much of the sun's surface. Like faculae they represent enhanced emission, and changes in their numbers could add up to significant changes in the solar output. We shall see, however, that AR faculae and QS network fields contribute to irradiance fluctuations differently.

As the sun rotates a feature on its surface is viewed at different angles. The contrast of sunspots is not strongly correlated with viewing angle. AR faculae, however, have low contrast near disk center but appear brighter near the limb. The nature of this center-limb variation is related to the structure of the flux tubes making up the facular elements. For example, the model of a facula as an evacuated flux tube with hot walls and a cool floor can account for much of the observed contrast variation, especially if allowance is made for the effect of a range of flux tube sizes [Spruit, 1976].

The center-limb variation of contrast also is used to estimate the contributions of

faculae to irradiance changes by means of "proxy" measures like the associated Calcium plage area. The fractional change in irradiance can be written [Chapman and Meyer, 1986]

$$\frac{\Delta S}{S} = c_p A_p \mu \phi(\mu) C(\mu) \qquad (1)$$

Here c_p is a calibration constant, A_p is the observed Ca plage area of a region, $\phi(\mu)$ describes the quiet sun photospheric limb darkening, and $C(\mu)$ describes the dependence of facular contrast on $\mu = \cos\theta$, where θ is the heliocentric angle between the plage and the disk center. The factor μ in Eq. (1) accounts for foreshortening as one approaches the limb. The facular contribution to solar luminosity fluctuations is the integral of the facular excess radiation pattern over the 2π steradians of the solar "sky"

$$\frac{\Delta L}{L} = (\frac{1}{2}) c_p A_p \int_0^1 \phi(\mu) C(\mu) \mu \, d\mu \qquad (2)$$

Most empirical models of facular contrasts have been zero or slightly positive at disk center [Hoyt and Eddy, 1982; Sofia, et al., 1982; Schatten, et al., 1985; Lawrence and Chapman, 1988] although some have used negative disk center contrast [Foukal, 1981]. Measurements of facular contrast at the disk center have yielded positive values, though these are quite low [Hirayama, et al., 1985; Lawrence 1988] or have been made at wavelengths near the H^- opacity maximum around 8600 Å [Lawrence, et al. 1988; Jones, 1992]. A recent study [Chapman, et al, 1992] matched photometric measurements of sunspot irradiance deficits and of Ca plage areas to ACRIM measurements made while an AR crossed the solar disk. This gave a best fit facular contrast function with high contrast near the limb but with a disk center contrast of about -1%. This decreases the estimated luminosity change of Eq. (2) by about 10%.

Since 1988 photometric observations have been made with the Lockheed tunable

filter instrument at the Swedish Solar Observatory at La Palma. These include very high resolution, nearly simultaneous, line-of-sight magnetic field and narrow band, mid-visible, intensity images of active regions covering heliocentric angles between 2° (near disk center) and 46°. Facular pixels gave contrasts near -3% at disk center, turning positive at a heliocentric angle near 20° [Topka, et al., 1992]. New Lockheed observations reported here confirm that disk center AR facular contrasts at visible wavelengths are negative. Similar San Fernando Observatory (SFO) observations yield the same conclusion. However, observations of QS network fields at Lockheed, at SFO, and also at the National Solar Observatory at Kitt Peak (NSO/KP) indicate that the associated contrasts are positive at disk center. Different contrast functions $C(\mu)$ apply to the AR and QS cases.

Observations at Lockheed, at SFO, and at NSO/KP further indicate that disk-center facular contrasts are color dependent. This may follow from color dependence of the opacity of the solar atmosphere due to the H^- ion and may thus be determined by the depth in the solar atmosphere to which one is able to see in different colors [Foukal and Duvall, 1985]. This is important for modelling facular atmospheres and for calibration of monochromatic ground-based observations with bolometric spacecraft observations.

In the next section we describe the instrumentation and data sets obtained at the three observatories which we employ in this paper. Then the results of analysis of the data are presented. Finally the results are discussed and conclusions drawn from them.

OBSERVATIONS

The Lockheed data were obtained at the Observatorio del Roque de los Muchachos, La Palma, Spain, using the 50 cm Vacuum Tower Telescope of the Swedish Solar Observatory [Scharmer, et al., 1985] and the Lockheed tunable filter instrument [Title, et al., 1992]. This instrument consists of a high-speed steering mirror for image stabilization,

reimaging optics, a polarization analyzer, a blocking filter wheel, a narrow bandpass (75 mÅ) tunable filter, and a 1024 × 1024 pixel CCD camera. Only 512 × 512 pixels were recorded, however, usually from the center of the CCD. This kept the data cycle to only about 3 sec per image. The scale was adjusted in different images from 0.137"/px to 0.166"/px to 0.274"/px corresponding to fields of view 70", 85" and 140", respectively. Each observing sequence had in common the following: one left- and right- circularly polarized pair in Fe I 6302 Å for longitudinal magnetograms, a five point line scan (-90, -30, 0, +30, +90 mÅ) in Fe I 5576 Å or Ni I 6768 Å for Dopplergrams, or a longer scan in Fe I 6302 Å for the determination of Stokes V, and at least one frame in the "continuum." In the Lockheed data a search was made within ~ 1 Å of the magnetic line center for a spectral interval with full width at half maximum (FWHM) = 75 mÅ as line-free as possible to be used for the continuum measurement. For the 6302 Fe line this was at -350 mÅ from line center; for the green lines it was -750 mÅ from line center. Exposure times were typically 0.2 sec. Practically, the resolution limit is about twice the pixel scale. For the La Palma observations, the resolution for magnetograms was > 0.5" and slightly better for the intensity images.

The products of interest here are co-registered images of line-of-sight magnetic field and of "continuum" intensity. For detailed data reduction procedures see Topka, et al. [1992]. Salient features of the data reduction are the following. Time intervals with excellent seeing were selected for each observation. The raw CCD images were corrected for pixel-to-pixel gain variations, for dark current, and flaws. The magnetograms were formed from the blue wing images of the 6302 Å line. Because these were not simultaneous with the "continuum" images, the two had to be numerically co-registered across the field of view, usually to an accuracy of a fraction of a pixel (estimated at 0.1"). The continuum images were corrected for any large-scale variations remaining in the flat field. Each image was

divided into 1 to 4 sub-images, depending on the nature of the fields in each. The mean heliocentric angle is determined for each facular area by comparison to the Mt. Wilson full-disk sunspot drawings for that day. The estimated accuracy is 0.25° at disk center and 0.5° at 40°. Table 1 indicates eight sets of observations included in the present study.

The SFO data were acquired with the 28 cm Vacuum Telescope and Vacuum Spectroheliograph operated in the Video Spectra-Spectroheliograph (VS^2HG) mode. Details of the instrumentation and data reduction may be found in Chapman and Walton, [1989] and Lawrence, et al., [1991]. The principal difference between these and the Lockheed data is that the CCD images are formed in two circular polarizations with a spectroheliograph, so that one CCD axis represents the solar EW direction with scale 0.46"/px and the other axis represents the spectral dimension with scale 8.8 mÅ/px. The observed spectral range included the Fe I 6302.5 Å magnetic line, a telluric O_2 line at 6302.0 Å and a telluric O_2 line at 6302.8 Å which is sometimes blended in the umbrae of sunspots. The solar NS direction is scanned by moving the spectrograph slit across the solar image. The scale in the NS direction is set by the scanning rate and has varied from 0.43"/px to 0.83"/px. The resulting data "cube" can be reduced to different kinds of spatial maps by appropriate operations on the spectral dimension. A "continuum" image was formed from the average of 5 adjacent pixels at 6302.25 Å. A line-of-sight magnetic image was formed from the first moment of the Stokes V profile of the magnetic line about the center of the I profile; the noise level is ~ 40 G. In this procedure corresponding pixels in the different images are simultaneous and co-registered; no de-stretching is required. The effective resolution for these data is > 1". The field of view is about 200" EW and variable NS depending on the scan speed and duration. Location of features on the solar disk is determined from the suitably rotated sunspot drawings in the Solar Geophysical Data Bulletin to an accuracy of 1° near disk

center and 2° at 40°. Table 2 indicates seventeen sets of SFO observations included in the present work.

The new NASA/NSO Spectromagnetograph [Jones, et al. 1992] is now in operation with the NSO/Kitt Peak Vacuum Telescope [Livingston, et al., 1976]. Data analysis techniques associated with it are described by Jones [1992]. The data are similar in concept to the SFO data in that a (spatial × spatial × spectral) data cube is formed in two circular polarizations, and that these can be reduced to various kinds of spatial maps, such as continuum intensity and line-of-sight magnetic field. The ability to choose different spectral regions for analysis is much greater than at SFO. Here we have included data in the visible at 5507 Å and 6122 Å and in the near IR at 8688 Å. For the Kitt Peak data, the "continuum" was taken as the average of the two extreme pixels at each end (i.e. 4 pixels total) of the overall spectral interval. The average distance of these from the line center was, for the 5507 Å line, 1.5 times the line FWHM, for the 6122 Å line, 1.9 times the line FWHM, and for the 8688 Å line between 1.4 and 1.9 times the line FWHM. The 8688 Å results were insensitive to the variation. The pixel scale is 1.14"/px, so the resolution is typically > 2". The field of view is the full solar disk.

NSO/Kitt Peak data included in this study are full-disk continuum and line-of-sight magnetic field images made at 6122 Å on 22 November 1991; at 8688 Å on 7 October 1991, 16 January 1992 and 3, 4 April 1992; and at 5507 Å on 9, 10, 14, 30 June 1992.

RESULTS

The contrasts we refer to are the observed percentage excess (or deficit) intensities of given image pixels over the average intensity of defined background pixels: $C_i = 100 \times (I_i - \langle I \rangle)/\langle I \rangle$. The contrasts are measured in some specified wavelength band which we refer to as "continuum." For each of the three data sets discussed, this and the

background pixel population are defined differently. Because the chosen wavelength bands are not far from magnetic lines, this is not really a continuum contrast. Neither is it white light. The goal, of course, is to represent the bolometric irradiance change, so this measure should be typical of the spectrum as a whole. A survey of the spectrum indicates a large number of lines of various kinds [Kurucz, 1991]. Thus some line contamination of the measurement may be to the good (we believe it probably less than 5%); certainly pure continuum would be atypical. Our use of the term "continuum" should be understood with this in mind.

From the magnetic and intensity images, we classify the continuum pixels according to their field strength. Field "free" pixels are used to define the QS photospheric level. Then intensities are converted to relative contrasts and these plotted versus field strength. Fig. 1 demonstrates this process for Lockheed observations of three ARs. The average intensity in the lowest magnetic bin (-12.5 G to 12.5 G) defines the background level. The facular areas at 3° and 17° from disk center show negative contrasts for all field strengths and thus have a negative overall contrast. The region at 40° from disk center has positive contrasts at most field strengths and overall.

Fig. 2 depicts a corresponding analysis of SFO data. For illustrative purposes, all data points in the range $10° \leq \theta \leq 20°$ were included from the 2nd and 3rd regions in Table 2. Shown are contrasts versus line-of-sight magnetic field in 20 G bins, together with the fraction of pixels populating each magnetic bin. The pixels are strongly clustered in the first three bins ($B < 60$ G), and we use the weighted average of these bins to determine the QS background level. At a magnetic field above 420 G both the pixel contrasts and the magnetic bin populations decrease rapidly. For consistent comparison of the Lockheed and SFO observations we follow Topka, et al. [1992] in interpreting the pixels beyond this "knee" as

representing micropores and in excluding them from calculations of overall contrast. As shown in Fig. 1, for the Lockheed data the knee occurs above 600 G. The overall contrast for the pixels in Fig. 2 is the weighted average over the range 60 G $\leq$ B $\leq$ 420 G. This gives a slightly positive value in this case.

Fig. 3 shows the result of several Lockheed determinations of overall facular contrast for a number of ARs versus heliocentric angle. Each data point includes magnetic fields in the range 188 G < B < 612 G. Below 188 G the points reflect a mixture of B signal with non-magnetic noise. At 100 G the mixture is about 50%. Since all the bins in Fig. 1 for θ = 3° and 17° have negative contrast, the exclusion of pixels below 188 G cannot change the signs of the overall average contrasts. The data points in Fig. 3 represent measurements made at different wavelengths, with different image scales and under different conditions of seeing and stray light. All of these will affect the magnitudes, but not the signs, of the average contrasts to some degree. No corrections have been applied; plots like Figs. 3 and 4, showing contrast averaged over magnetic field, have this built-in uncertainty. As was found in Topka, et al. [1992], the AR contrasts near the disk center are negative, crossing to positive at an angle of about 20°.

Fig. 4 gives a similar analysis of SFO data. The active regions in Table 2 were divided into 5° bins of heliocentric angle, and then overall facular contrasts for 60 G < B < 420 G were calculated for each image in each bin. Also shown are averages over a consolidation of all the images, in 10° bins of θ. A linear regression line has been plotted through these points. The dark AR facular contrasts near disk center, found in the Lockheed data, appear also in the SFO data.

We have also observed disk center contrasts associated with scattered QS network fields, as opposed to AR faculae. This is illustrated for θ = 2° for the Lockheed data in

Fig. 5. The contrast versus magnetic field plot starts negative, but then turns positive at 200 G and remains positive until nearly 500 G. This is markedly different behavior from the near-disk-center AR facular contrast curve which is plotted for reference.

The overall mean contrast is +0.68% for all pixels at 150 G and above. The statistical error is ± 0.05%, but the uncertainty due to definition of the background level is probably closer to ± 0.2%. This weighted mean is dominated by the peak in contrast occurring near 350 G. Above 475 G the contrast is negative due to the presence of 3 micropores within the field of view. These data, however, total only 59 pixels so they contribute little to the weighted average. Between 150 G and 200 G there are nearly 900 pixels, enough to contribute significantly to the weighted mean, but the contrast is very small.

As shown in Table 2, five observations have been made at SFO of disk center network. The contrast versus magnetic field for the aggregate of these observations is shown in Fig. 6 along with the magnetic bin occupation fractions. Essentially all of the magnetic bins show positive contrast. The overall contrasts for each of the five images are also shown in Fig. 4 together with the overall average contrast for all the network pixels. Fig. 6 also illustrates the contrasts and bin populations for the aggregate all of the AR observations within 10° of the disk center. These give a negative overall contrast represented by the leftmost open square point in Fig. 4. The disk center contrast of QS network elements are greater than those of AR faculae to a high level of statistical significance.

Data similar to the Lockheed and the SFO data have been acquired also at NSO/KP with the new NASA/NSO Spectromagnetograph. Several sets of full-disk continuum and line-of-sight magnetic field maps were made, as listed above, at 8688 Å in the near IR. These data yielded positive facular contrasts at essentially all magnetic field strengths and

at all disk positions. This result matches earlier SFO measurements of positive contrasts at 8640 and 8680 Å [Lawrence, et al., 1988]. NSO/KP observations also have been carried out in the mid-visible at 5507 and 6122 Å. These give negative contrasts at some magnetic field strengths and positive contrasts at others. Fig. 7 presents some of these contrasts for various magnetic bins and in 5° bins of θ. In Fig. 8 the data between $0° \leq \theta \leq 20°$ are combined and plotted versus line-of-sight magnetic field. These observations parallel the Lockheed and SFO observations shown in Figs. 5 and 6. When differences in resolution are taken into account, this result is quite consistent with the Lockheed and the SFO observations of disk center QS network. The NSO/KP observations were made when no large ARs were near the disk center, so they are basically network observations.

DISCUSSION

SFO observations of AR faculae yield a contrast versus line-of-sight magnetic field dependence which is virtually identical to that of Topka, et al. [1992]. Any discrepancies can be attributed to differences in resolution. Negative disk center contrasts were found at SFO for facular pixels defined to have field strengths between 60 and 420 Gauss. Analysis of Lockheed observations of three additional active regions with heliocentric angles 3°, 17° and 40° further confirms the dark disk center active region facular contrasts.

A surprising result comes from observations of disk center, QS network, as opposed to AR faculae. One such observation has been carried out with the Lockheed instrument and five at SFO. In each case the average magnetic pixel contrast is more positive than the corresponding AR contrast. The Lockheed/La Palma case is illustrated in Fig. 5 and a composite of the five SFO cases is shown in Fig. 6. Fig. 8 shows a summary of NSO/KP observations of the near disk center made at 6122 Å on 22 November 1991 and at 5507 Å on 9, 10, 14 June 1992. These QS network results match those from Lockheed and SFO.

These results have a number of implications. First, estimates of irradiance and luminosity variability from measured magnetic field areas depend strongly on facular center-limb contrast functions. See Eqs. (1) and (2) above. Those who wish to model the facular contributions to solar variability both on the active region and the solar cycle time scales [see, for example, Foukal, et al., 1991] may need to use different center-limb contrast functions for the AR faculae and QS network. We estimate that differences ~100% in the estimated irradiance variation could ensue from this.

Second, Figs. 5 and 6 show that the magnetic pixel distributions for the QS network fall off rapidly with magnetic signal and truncate at low field levels: about 500 G for the Lockheed data and about 250 G for the SFO data. However, the AR distributions from both data sets show long, well-populated tails of dark pixels extending to much higher field strengths. These represent the dark features we have called micropores. In the aggregate they account for a large fraction of the magnetic flux in the AR faculae. If included in the calculation they would make a substantial negative contribution to the overall contrast.

This result exhibits a remarkable difference between the fundamental make-ups of the QS network and AR faculae. In particular, micropores are almost completely lacking in the network, but are quite numerous in faculae. Micropores are the darkest component of AR faculae at disk center, but they may be the brightest component at the limb [Knölker and Schüssler, 1988]. Since the network is essentially free of micropores, AR faculae may be brighter at the limb, on average, than QS network.

Our micropores appear identical to the "invisible sunspots" reported by Zirin and Wang [1992] and perhaps are related to the "magnetic knots" of Beckers and Schröter [1968]. Zirin and Wang reported the presence of invisible spots in network fields far from ARs. A few micropores appear in the QS Lockheed image. However, these were localized

in a small area of relatively strong field. This may indicate the presence of small, scattered patches of "enhanced" network not associated with ARs.

The brighter disk center emission of QS network versus AR faculae also may stem from differing flux tube orientations. The more closely packed AR flux tubes may be more closely and more vertically aligned. The more loosely packed QS flux tubes may be observed at a variety of inclination angles, and thus of effective center-limb distances. Those seen at inclination angles above 20° should appear bright rather than dark. This interpretation is supported by the recent observations of Murray [1992], who found inclination angles of up to 45° in weakly magnetic areas, but much less in stronger field areas.

Joint observations like those presented here may reveal different features due to differing spatial resolution. For example, the Lockheed observation of the QS network (Fig.5) shows a dip in contrast between 0 G and 200 G that is not present in the SFO observations (Fig. 6). Statistical analysis indicates that the dip is real, rather than an artifact of the Lockheed data. It is present in both the AR and QS network data in Fig. 5. The dip must be due to a small and local phenomenon which is resolved in the Lockheed observations but not in the SFO observations. This may constrain models of small flux tubes, which must be able to correctly predict both the Lockheed and the SFO results.

A study of facular contrasts near 8688 Å [see also Jones 1992] has indicated positive contrasts near disk center. This is in agreement with earlier measurements by Lawrence, et al. [1988] at 8640 Å and 8680 Å. These wavelengths are near the H^- opacity maximum, and their difference from the mid-visible, lower opacity, results may represent a depth effect. Facular contrasts near 1.6μ at the H^- opacity minimum are dark near disk center [Worden, 1975; Foukal, et al., 1989, 1990]. This suggests that contrasts at various wavelengths may correlate positively with H^- opacity. For visible wavelengths, the opacity increases with

wavelength, so one can hypothesize that disk center contrast should increase with wavelength in the visible range. This is indeed the case for Lockheed observations in three colors of a single AR near heliocentric angle 3°. Over a range of magnetic field strengths from 0 to 600 G, corresponding to facular emission, the contrasts increase in the order of increasing wavelength, with the 5576 Å contrast nearer the 5250 Å than the 6302 Å. This is demonstrated in Fig. 9 for contrasts corrected for location on the Planck curve. This indicates a facular effective temperature about 20 K higher in the red at 6302 Å than in the green at 5250 Å. This in turn indicates that the radiation is emitted from different heights in the solar atmosphere.

The above work indicates the value of measurements at many wavelengths across the spectrum. This would allow a bolometric calibration of various monochromatic facular proxy measures. At the same time, knowledge of facular contrasts as a function of H^- opacity and hence atmospheric depth would provide important information for construction of models of facular structure.

ACKNOWLEDGMENTS

The San Fernando Observatory work reported here was supported in part by NSF Grants ATM-8817634 and ATM-9115111 and NASA grant NAGW-3017. JKL expresses gratitude to Drs. Gary Chapman and Stephen Walton. The development of the Lockheed tunable filter instrument and the execution of 4 successful observing runs at the Swedish Solar Observatory, La Palma, reflect the efforts of many people. KPT especially thanks Drs. Alan Title, Theodore Tarbell, Richard Shine, and Göran Scharmer. At the SSO he thanks Rolf Kever, Paco Armas, and Göran Hosinsky. At Lockheed he thanks Dexter Duncan, Christopher Edwards, Zoe Frank, Kathy Hwu, Michael Levay, Michael Morrill, Roger Rehse, William Rosenberg, Kermit Smith, and Darrel Torgerson. This work was supported by Lockheed Independent Research Funds, by NASA contracts NAS8-32805 (SOUP), NAS5-26813 (OSL), NAS5-30386 (MDI), and NAS8-38106 (BSOUP), and NSF contract ATM-8912841. The National Solar Observatory (NSO) is a division of the National Optical Astronomy Observatories (NOAO), which is operated by the Association of Universities for Research in Astronomy, Inc. under cooperative agreement with the National Science Foundation. The NSO/KP Vacuum Telescope is operated cooperatively by NOAO/NSO, NASA/GSFC, and the National Oceanic and Atmospheric Administration's Space Environment Laboratory (NOAA/SEL).

REFERENCES

Beckers, J.M. and E.H. Schröter, The intensity, velocity and magnetic structure of a sunspot region I: observational technique; properties of magnetic knots, Solar Phys., 4, 142, 1968.

Chapman, G.A., A.D. Herzog, J.K. Lawrence, S.R. Walton, H.S. Hudson and B.M. Fisher, Precise, ground-based, solar photometry and variations of total irradiance, J. Geophys. Res., 97, 8211, 1992.

Chapman, G.A. and A.D. Meyer, Solar irradiance variations from photometry of active regions, Solar Phys., 103, 21, 1986.

Chapman, G.A. and S.R. Walton, Recent results from the San Fernando Observatory video spectra-spectroheliograph, in High spatial resolution solar observations, edited by O. van der Luhe, p. 402, Sacramento Peak Observatory, Sunspot, NM, 1989.

Foukal, P., Sunspots and changes in global properties of the sun, in Physics of Sunspots, edited by L.E. Cram and J.H. Thomas, p. 391, Sacramento Peak Observatory, Sunspot, NM, 1981.

Foukal, P. and T. Duvall, Jr., Differential photometry of magnetic faculae, Astrophys. J., 296, 739, 1985.

Foukal, P., K. Harvey and F. Hill, Do changes in the photospheric magnetic network cause the 11 year variation of total solar irradiance?, Astrophys. J., 383, L89, 1991.

Foukal, P., R. Little, J. Graves, D. Rabin and D. Lynch, Infrared imaging of faculae at the deepest photospheric layers, Astrophys. J., 353, 712, 1990.

Foukal, P., R. Little and J. Mooney, Infrared imaging of sunspots and facular at the photospheric opacity minimum, Astrophys. J., 336, L33, 1989.

Hirayama, T., S. Hamana and K. Mizugaki, Precise wideband photometry of photospheric

faculae with an emphasis on the disk center, Solar Phys., 99, 43, 1985.

Hoyt, D.V. and J.A. Eddy, An atlas of variations in the solar constant caused by sunspot blocking and facular emission from 1874 to 1981, Tech. Note TN-194, Natl. Cent. for Atmos. Res., Boulder, CO, 1982.

Hudson, H.S., Observed variability of the solar luminosity, Annu. Rev. Astron. Astrophys., 26, 473, 1988.

Jones, H.P., T.L. Duvall, Jr., J.W. Harvey, C.T. Mahaffey, J.D. Schwitters and J.E. Simmons, The NASA/NSO spectromagnetograph, Solar Phys., 139, 211, 1992.

Jones H.P., New solar cycle data from the NASA/NSO spectromagnetograph, The Solar Cycle, edited by Karen L. Harvey, Astronomical Society of the Pacific Conference Series No. 27, 315, 1992.

Knölker, M. and M. Schüssler, Model calculations of magnetic flux tubes IV. Convective energy transport and the nature of intermediate size flux concentrations, Astron. Astrophys., 202, 275, 1988.

Kurucz, R.L., The solar spectrum, in Solar Interior and Atmosphere, edited by A.N. Cox, W.C. Livingston and M.S. Matthews, p. 663, University of Arizona Press, Tucson, 1991.

Lawrence, J.K., Multi-color photometric observations of facular contrasts, Solar Phys., 116, 17, 1988.

Lawrence, J.K. and G.A. Chapman, Photometric observations of facular contrasts near the solar limb, Astrophys. J., 335, 996, 1988.

Lawrence, J.K., G.A. Chapman and A.D. Herzog, Photometric determination of facular contrasts near the solar disk center, Astrophys. J., 324, 1184, 1988.

Lawrence, J.K., G.A. Chapman and S.R. Walton, Weak magnetic fields and solar irradiance

variations, Astrophys. J., 375, 771, 1991.

Livingston, W.C., J. Harvey, A.K. Pierce, D. Schrage, B. Gillespie, J. Simmons, and C. Slaughter, Kitt Peak 60 cm vacuum telescope, Applied Optics, 15, 33, 1976.

Murray. N., On the inclination of photospheric solar magnetic fields, Astrophys. J., 401, 386, 1992.

Scharmer, G.B., D.S. Brown, L. Pettersson and J. Rehn, Concepts for the Swedish 50 cm vacuum solar telescope, Appl. Optics, 24, 2558, 1985.

Schatten, K.H., N. Miller, S. Sofia, A.S. Endal, G.A. Chapman and J. Hickey, The importance of improved facular observations in understanding solar constant variations, Astrophys. J., 294, 689, 1985.

Sofia, S., L. Oster and K.H. Schatten, Solar irradiance modulation by active regions during 1980, Solar Phys., 80, 87, 1982.

Spruit, H.C., Pressure equilibrium and energy balance of small photospheric fluxtubes, Solar Phys., 50, 269, 1976.

Title, A.M., K.P. Topka, T.D. Tarbell, W. Schmidt, C. Balke and G. Scharmer, On the differences between plage and quiet sun in the photosphere, Astrophys. J., 393, 782, 1992.

Topka, K.P., T.D. Tarbell and A.M. Title, Properties of the smallest solar magnetic elements I. Facular contrast near sun center, Astrophys. J., 396, 351, 1992.

Willson, R.C., S. Gulkis, M. Janssen, H.S. Hudson and G.A. Chapman, Observations of solar irradiance variability, Science, 211, 700, 1981.

Worden, S.P., Infrared observations of supergranule temperature structure, Solar Phys., 45, 521, 1975.

Zirin, H. and H. Wang, Detection of "invisible sunspots," Astrophys. J., 385, L27, 1992.

FIGURE CAPTIONS

1. Average pixel contrast versus line-of-sight magnetogram signal in 25 G bins for all image pixels from 3 La Palma observations of active region faculae. The field of view is approximately 80" × 80"; the mean heliocentric angle of each observation is 3° (O), 17° (▲), and 40° (■). Error bars give the 1 σ statistical error of each measurement; when not visible they are smaller than the symbol.

2. Average pixel contrast (O) versus line of sight magnetic field in 20 G bins for all pixels between heliocentric angles $10° \leq \theta \leq 20°$ in two SFO images taken at 6302 Å on 17 Aug 1989. Also shown (□) on the same scale is the logarithm of the fraction of pixels in each magnetic bin.

3. Pixel contrast, averaged from 188 G to 612 G, versus heliocentric angle. The smooth curve is a quadratic fit to La Palma observations of the 7 active regions listed in Table 1. The wavelengths are (O) 5250 and 5576 Å, (▲) 6768 Å and (□) 6302 Å. The solid square (■) gives the overall contrast of QS network elements near disk center. Statistical error bars are smaller than the symbols.

4. SFO pixel contrast, averaged from 60 G to 420 G, versus heliocentric angle. (O) single AR images in 5° bins. (□) averages over all AR images in 10° bins; a linear regression line is plotted for these points. (●) QS network contrast measurements. (■) weighted average for all network images. Error bars give 1σ statistical uncertainties when larger than the symbols.

5. (O) average pixel contrast versus line-of-sight magnetogram signal in 25 G bins for faculae in the AR nearest the disk center (3°). (●) contrast versus magnetogram signal in 50 G bins for disk center network. Logarithms (shifted down by 3 for clarity) of the fractions of pixels found in each bin: (□) for AR and (▪) for disk center QS network.

6. (O) average pixel contrast versus line of sight magnetic field in 20 G bins of all SFO AR observations with heliocentric angle $0° \leq \theta \leq 10°$. (●) the same for all five observations of QS network near the disk center. Shown on the same scale are the logarithms of the fractions of pixels found in each bin for the (□) AR and (▪) network cases.

7. Average pixel contrast versus heliocentric angle in five degree bins for Kitt Peak measurements in various magnetic bins: (O) λ5507, 4-16 G; (▲) λ5507, 16-28 G; (◊) λ5507, 28-100 G; (●) λ6122, 60-160 G; (♦) λ6122, 180-260 G. The 5507 Å images were made on 9, 10, 14 June 1992, and the 6122 Å image on 22 November 1991.

8. Average pixel contrast versus magnetic field in various bins for heliocentric angle $\theta \leq 20°$. (●) data at 6122 Å and (O) data at 5507 Å.

9. Average pixel contrast versus line-of-sight magnetogram signal in 25 G bins made at (O) 6302 Å, (●) 5576 Å, and (▪) 5250 Å. The AR is at $\theta = 3°$, and the different wavelength images are simultaneous within 6 s. If the AR faculae were a perfect blackbody radiator the plots would all coincide.

TABLE 1. Solar Active Regions Observed at La Palma

Target NOAA	θ Min	θ Mean	θ Max	Date	Time (UT)	Scale ("/pixel)
AR 6085	2.3	4.8	7.4	06-06-90	08:25	0.137
AR 5168	10.7	13.7	16.7	09-29-88	10:07	0.166
AR 6086	21.4	27.4	33.7	06-07-90	07:57	0.274
AR 5572	37.4	42.0	47.0	07-03-89	09:15	0.137
AR 6774	0.6	3.2	7.3	08-14-91	10:13	0.166
AR 6766	13.0	16.7	20.7	08-10-91	11:46	0.166
AR 6774	35.7	40.0	44.5	08-11-91	10:05	0.166
QS	0.0	2.0	3.6	08-10-91	17:18	0.166

TABLE 2. Solar Active Regions Observed at SFO

Target NOAA	θ(Deg) Min	θ Max	Date	Time (UT)	Scale("/px) NS × EW
AR 5643	5	10	08-17-89	18:10	0.83 × 0.46
AR 5643	5	25	08-17-89	18:11	0.83 × 0.46
AR 5643	0	20	08-17-89	22:59	0.83 × 0.46
AR 5643	10	30	08-18-89	22:43	0.83 × 0.46
AR 5643	20	40	08-19-89	20:12	0.83 × 0.46
AR 5643	30	55	08-20-89	11:46	0.83 × 0.46
AR 5643	40	70	08-21-89	20:12	0.83 × 0.46
AR 5669	20	35	09-05-89	19:54	0.43 × 0.46
AR 5669	20	35	09-05-89	19:55	0.43 × 0.46
AR 6309 6311 6312	5	15	10-12-90	20:09	0.43 × 0.46
AR 6309 6311 6312	5	15	10-12-90	20:11	0.43 × 0.46
AR 6734 6744	15	30	07-26-91	21:56	0.43 × 0.46
QS	0	10	07-06-92	16:43	0.43 × 0.46
QS	0	10	07-06-92	16:44	0.43 × 0.46
QS	0	10	08-22-92	18:25	0.43 × 0.46
QS	0	10	08-22-92	18:26	0.43 × 0.46
QS	0	10	08-22-92	18:29	0.43 × 0.46

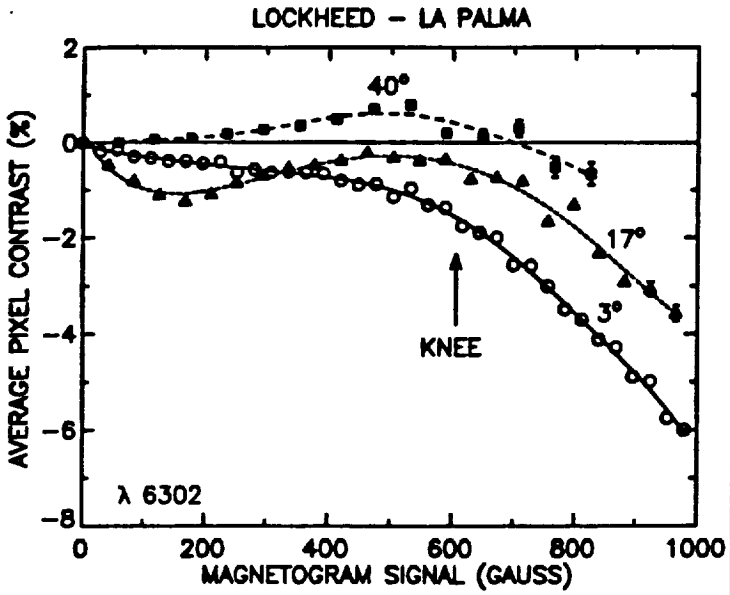

Fig. 1

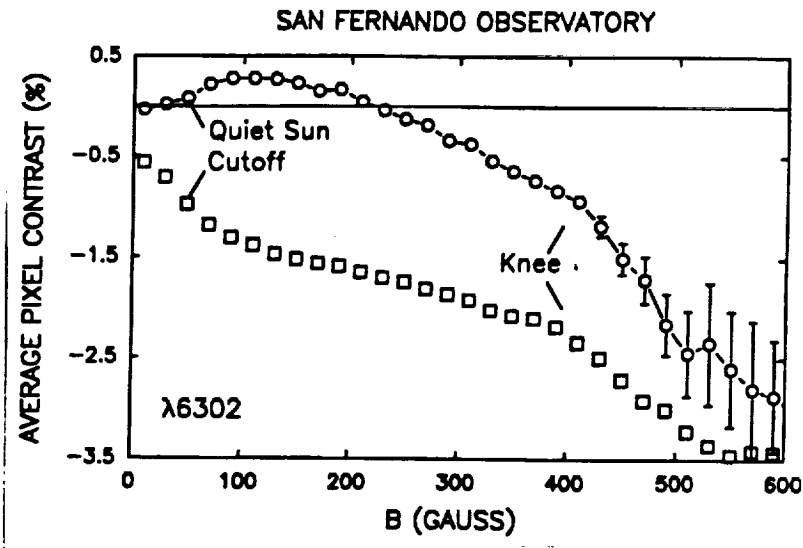

Fig. 2

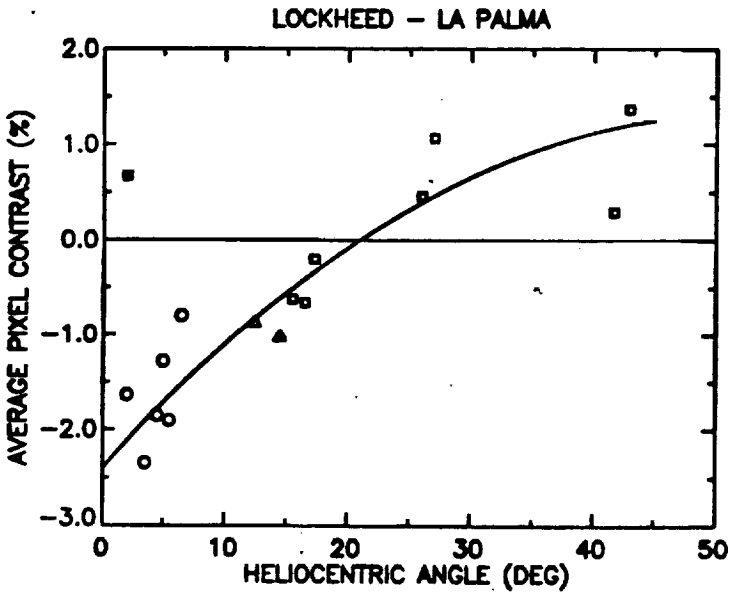

Fig. 3

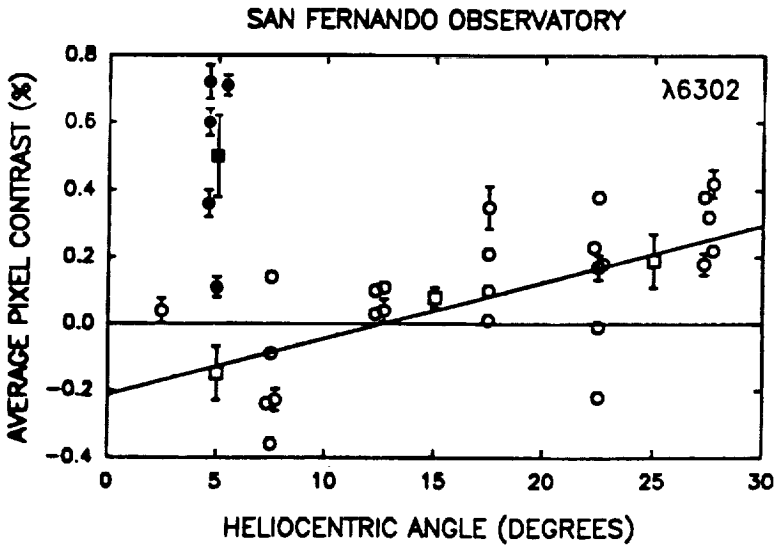

Fig. 4

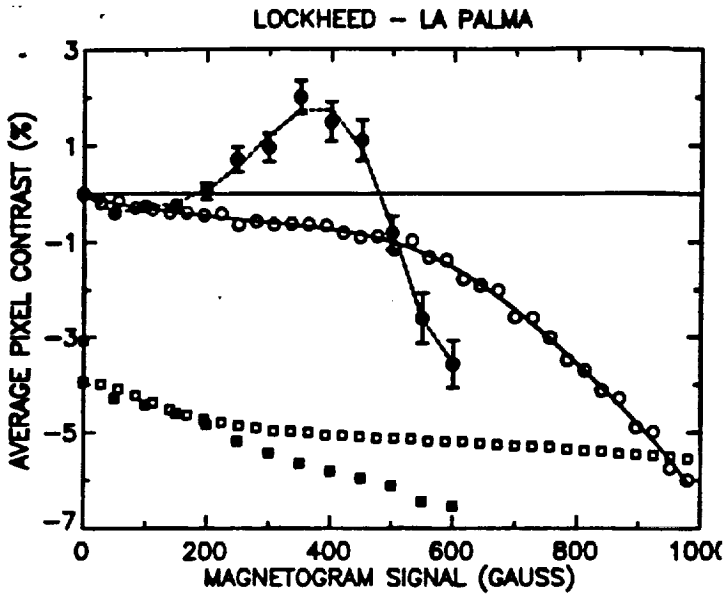

Fig. 5

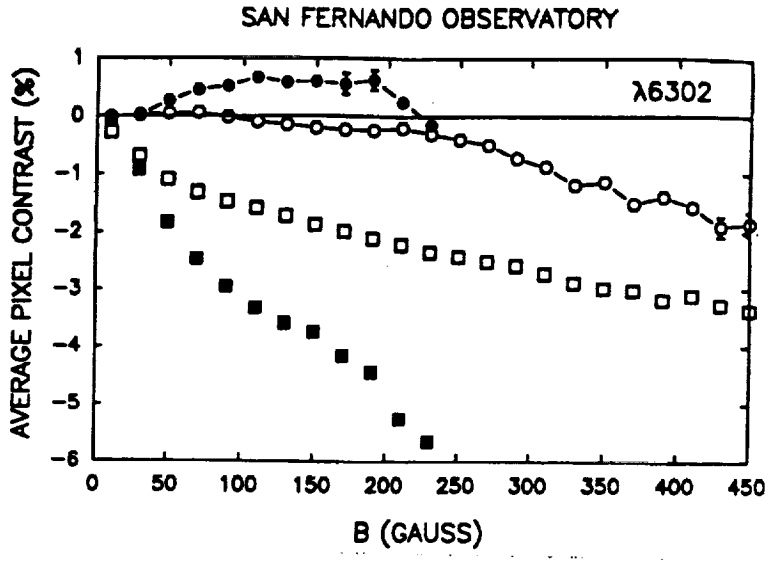

Fig. 6

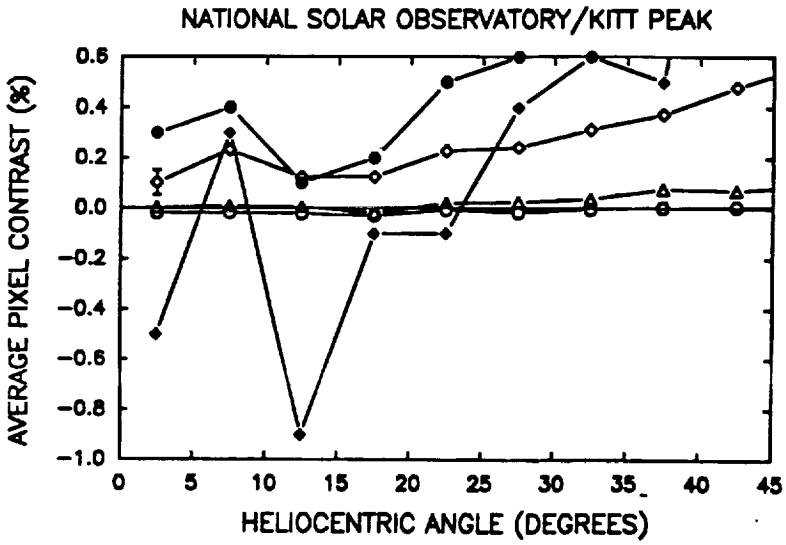

Fig. 7

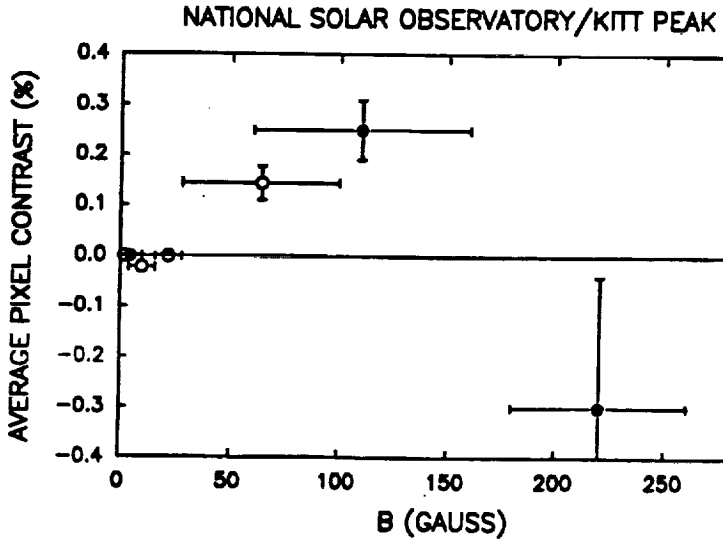

Fig. 8

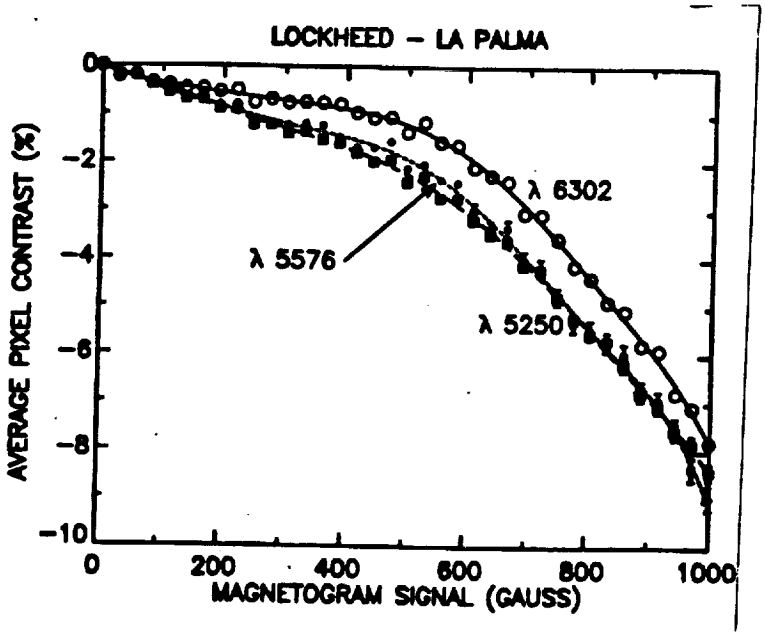

Fig. 9

Appendix C: Poster Paper from the AGU Meeting, December, 1992

Simultaneous Observations of Flares in the Solar Photosphere, Chromosphere, and Corona from La Palma and Yohkoh.

T.D. Tarbell, L.W. Acton, Z.A. Frank, R.A. Shine,

A.M. Title and K.P. Topka (Lockheed Palo Alto Research

Laboratory)

Paper presented at
AGU Meeting, Dec. 1992

From May 1 to July 6, 1992, we collected observations of active regions with the SOUP/CIP tunable filter instrument at the Swedish Solar Observatory on La Palma, coordinated with the X-ray telescopes on Yohkoh. The ground-based observations consisted of high-resolution movies of the photosphere in continuum, Fe lines, Doppler velocities, and longitudinal and transverse magnetograms; and of the chromosphere in multiple wavelengths of Hα, Na D, and Ca II K. Many flares were observed simultaneously with Yohkoh, the largest being an M9 on May 8 and an M2 on July 3. Other interesting phenomena observed this way were filament eruptions, emerging flux regions, and flare loops above the limb. The July 3 flare was observed completely in one Yohkoh orbit, with excellent seeing on La Palma. It showed a very gradual buildup phase lasting 45 minutes before the impulsive explosion in hard X-rays. The progress of reconnection in the corona during the buildup can be traced in detail by overlaying the H-alpha emission onto the magnetic footpoints in the photosphere with 0.5 arcsecond resolution. Initial examples of co-aligned images and movies are shown on video.

This work was supported by several NASA contracts, primarily NASW-4612 (La Palma observing) and NAS8-37334 (SXT).

1.0 Introduction

High resolution movies of the photosphere in active regions reveal fascinating flow fields and magnetic fine structures which are completely missed in low resolution or intermittent observations. Simultaneous chromospheric movies in the H_α, Na D, and Ca II K lines show a bewildering variety of dynamic features, some of which are clearly responses to the photospheric drivers. In 1992, we collected very high quality data of this type in coordinated observations with the coronal X-ray telescopes on Yohkoh. We plan to study the best of these movies to identify and characterize quantitatively, when possible, the photospheric origins of several well-known beasts in the zoo of upper atmospheric activity.

Excellent observations are available for emerging flux regions, active region growth, flares, spicules, Ellerman bombs, filaments, and sunspots. For example, we have a superb optical observation of an M2 flare, with H_α, vector magnetic, Na D, and Ca II K movies of the gradual buildup and impulsive phases with 0.5 arcsecond resolution. There are simultaneous Yohkoh observations of this entire event in hard and soft x-rays, which will be coaligned with our movies and compared. Other observations show the buoyant rise of tiny magnetic flux ropes through the continuum layer, photosphere, low chromosphere and eventually (we hope) into the soft x-ray corona. Frequent small flares, with obvious reconnections in the H_α fibril topology, are triggered by the emergence and proper motion of these new flux ropes.

Our data are time series of very high resolution digital images collected with narrowband tunable filters. The 0.05 Å SOUP filter isolates several photospheric and chromospheric lines in the 5000 – 7000 Å range. A 0.15 Å Ca II K line tunable filter is used for simultaneous chromospheric observations. The instrument is operated at two excellent solar telescopes, the Swedish Solar Observatory (SSO) on La Palma and the German Vacuum Tower Telescope (VTT) on Tenerife. Raw images are converted into coaligned digital movies of intensities, Doppler shifts, transverse velocities, and longitudinal magnetograms.

It is instructive (and humbling) to recall that raw data not unlike ours, high resolution movies of many different photospheric and chromospheric images, were first collected in the early 1970's, with the Universal Birefringent Filter at Sacramento Peak. Of course, those movies were on film, and so it proved impossible to compare wavelengths in detail or study them quantitatively. The advent of large digital array detectors, fast workstations, and inexpensive data storage has revolutionized high resolution solar physics. It is now possible to isolate, identify, and measure physical properties of these complex phenomena. In addition, we also have access to the X-ray movies of the corona through our Yohkoh colleagues. Several of our scientific programs are simply attempts to use these modern tools and data sets to understand the physics of dynamical features which were discovered and named generations ago.

Since we have more good quality data sets which deserve analysis than people to study them, we are eager to discuss collaboration with anyone willing to work on the data.

2.0 High Resolution Observations

Starting in August, 1988, we have had an observing run every summer at the 50 cm vacuum refractor of the SSO on La Palma. This telescope is known for its outstanding seeing: the highest resolution solar movie ever made is the result of applying LPARL image processing techniques to continuum observations obtained at SSO. Each of these five expeditions has collected very high quality time sequences of the type required for this proposal. Starting in 1989, we have operated our filtergraph every year in shorter runs at the German Vacuum Tower Telescope (VTT) on Tenerife, while scientists from the Kiepenheuer-Insitut für Sonnenphysik (KIS) observed simultaneously with their echelle spectrograph.

The purpose of our instrumentation is to collect very high resolution images in narrow wavelength bands and well-defined polarization states, with true spatial resolution down to 200 km on the sun. Polarization measurements produce the raw data for longitudinal and transverse magnetograms. Both vertical and horizontal velocities are measured using Dopplergrams and correlation tracking respectively. In the chromosphere, magnetic connectivity and energy release in flares and other transients are recorded in H_α images at several wavelength positions within the line. The ground observing instrument consists largely of engineering models and flight components of the SOUP instrument and the OSL CIP instrument.

The images are collected with two narrowband tunable filters, one for the mid-visible range and a second for the Ca II K line. Each uses a large-format digital CCD camera, with images recorded digitally on Exabyte tape. The visible filter system was built initially for SOUP and has been upgraded in some components for CIP. The passband is narrow enough (50-80 mÅ) to separate cleanly the core and wings of of Fe I lines in the photosphere for magnetic and velocity measurements. The CIP brassboard CCD camera with a TI-Japan uniphase detector is used with this filter. It takes 512×512 or 1024×1024 12 bit digital images and records them at a rate of one every 2.5 or 8 seconds continuously.

The Ca II K line filter was built using Lockheed Independent Research funds and is tunable across the line with 0.15 or 0.30 Å bandpass. It provides chromospheric intensity over a range of heights, for studies of wave propagation, chromospheric heating, and magnetic activity. It can be used with an OSL brassboard camera or with the SSO video CCD cameras, which digitize video frames selected for sharpness with optional integration to increase light levels. A third camera with a white light or broad band image is also digitized by the SSO system; this is exactly simultaneous with the Ca II image and can be used to remove seeing distortions from the narrowband image in subsequent processing.

The observing sequence is executed by a computer (IBM PC clone), which controls the tunable filter system and commands the exposure and readout of the CCD camera. The data from the CCD camera is collected on a Vaxstation 3200. The workstation displays the filter images on a video monitor and stores the digital images on tape. In 1992, we began recording videodisk movies of selected wavelengths in real-time. These movies have

proven extremely valuable for their instant feedback on evolution of the target region and the state of the instrument, as well as for choosing data sets to analyze afterwards.

A generic observing sequence for active region evolution might take a red continuum image, a circular polarization pair in Fe I 6302 Å for a longitudinal magnetogram, and five wavelengths spaced through H_α. This could run all day long with a field of view of 140 arcseconds square, a cadence of about 30 seconds, and a pixel size of 0.27 arcsecond. This mode uses the full CCD with 2 by 2 summing. When seeing is especially good, the summing can be suspended which yield pixels of 0.13 arcsecond. In order to maintain the cadence, the field of view is then usually restricted to the central 512 x 512 area of the CCD (field of view 70 arcseconds square). The field of view can be increased to 170 arc seconds or 210 arcseconds for very large regions or mediocre seeing.

In 1992, we spent most of our time at La Palma observing the same region as the Soft X-ray Telescope on Yohkoh. For this campaign, we adopted a specific observing strategy. During Yohkoh observing times, we ran movie sequences with good time resolution. During some of the spacecraft nights, we ran "context" sequences: extensive wavelength scans of Ha to show chromospheric connectivity; detailed Stokes polarimetry sequences for vector magnetograms; and wavelength scans of circular polarizations for more accurate magnetic field strengths. We also attempted to run context sequences in the late afternoon, for simultaneous comparisons with magnetograms from US observatories. Different movie sequences were available, optimized for different scientific programs such as flux emergence, impulsive events, flows at different heights, buildup of magnetic shear, etc.

The coordinated La Palma–Yohkoh observing was very successful this year. It lasted from May 1 to July 6, and several mornings had excellent seeing for periods of an hour or more; many full days of movies of the Yohkoh target region were obtained in good seeing. These contain joint observations with the x-ray telescopes of just about every type of dynamic phenomenon which occurs in solar active regions, except for a giant flare. Noteworthy observations were M flares on May 8, May 20, June 8 and July 3, the last observed in excellent seeing and fully coordinated; joint observations with the LPARL UV & X-ray rocket flight on May 12; excellent sunspot sequences on June 16 and July 2; quiet sun and an emerging flux region on June 30; buildup and shear of a large active region on June 22-25, leading to an X flare, which unfortunately occured just after La Palma and Yohkoh sunset. The limitations of solar observing from the ground and low earth orbit are still with us!

3.0 Flux Emergence and Active Region Growth

The emergence of new magnetic flux through the photosphere is the first step in the formation of an active region. We have several very good observations of young, rapidly growing regions. One can learn to recognize emerging flux in movies of raw data and then find emergence episodes throughout our movies of mature regions as well.

We obtained excellent observations on June 30, 1992, of a rapidly growing region near disk center. For two hours, the images have very good resolution (one-third arcsecond in the best frames). A comprehensive data set was taken, including photospheric continuum, Doppler, and longitudinal magnetic measurements; Na D Doppler and intensity measurements; H_α line center and wing images; and Ca K filtergrams. In the movies, one can see the steady progression of flux tubes rising through the continuum level, middle photosphere in the Fe lines, low chromosphere in Na D, and the wings of H_α, culminating in the formation of tiny arch filaments in the center of H_α. We plan to analyze some of these events to make definitive measurements of the buoyant rise of new flux tubes into the chromosphere, for comparison with theoretical models of this process, for example those of Tajima and his collaborators. Although this was not the Yohkoh target region, soft x-ray images are available every ten minutes or so to show the corona at coarser resolution. Oddly, this region was not very bright in x-rays in spite of the rapid flux emergence and H_α activity.

In every case we have seen, flux emergence does not take place at a neutral line separating polarities. Instead, it is occurring in small bipolar events spread over an area large compared with the size of the bipoles themselves at first appearance. Even a snapshot shows that the polarity mixing makes it impossible to draw a neutral line. Perhaps some of the rising flux ropes emerge in many places, like multiple loops of a sea serpent above the surface; careful study of the magnetic movie may confirm this. Some bipoles also emerge with axes at large angles (even right angles) to the main axis of the emergence. The movies show that the opposite poles of an emerging bipole separate and then move rapidly across the "neutral zone". Speeds up to 4 km/s are commonly seen in this initial proper motion. These exceed the normal horizontal flow speeds measured from granulation, and they appear to disagree in direction as well. These differences indicate the importance of magnetic buoyancy and tension forces and they should provide clues to the subsurface configuration of the emerging flux rope.

A very important consequence of this geometry is that many flux cancellation and reconnection events are forced to occur among the newly emerged magnetic elements. With opposite polarities moving in opposite directions through the same area, collisions are frequently observed. Sometimes dramatic reconnections of the H_α fibrils are seen when the magnetic footpoints of a set of fibrils are cancelled by intrusion of opposite polarities. This is very graphic evidence for magnetic reconnection taking place above the surface, presumably in the low chromosphere. These events are discussed further in the section on flares below.

4.0 Flares

On July 3, 1992, we obtained superb optical observations in excellent seeing of an M2 flare in region AR 7216 at N14 E28. The preflare, gradual buildup and impulsive phases were fully observed in one Yohkoh orbit, with all instruments performing well and all data recovered. Therefore, we will describe these observations in some detail and discuss some interesting coronal measurements which can be simply derived from the optical images. Figure 1 shows the GOES soft X-ray plot for this event.

The region was very large (more than 4 arcminutes E–W) and appeared rather simple and inactive in H_α. After context observations covering the whole region, we ran a movie sequence from 08:55 –09:49 UT; Yohkoh observing started at about 09:00. The movie sequence had 3 loops for 3 different time resolutions: H_α line center and far blue wing and longitudinal magnetograms every 30 seconds, 5 images spaced through the core of Na D every 60 seconds, and 5 more H_α wavelengths and a vector magnetic set every 120 seconds. Because of the excellent seeing, the movie used higher magnification, for a 112 arcsecond square field (0.22 arcsecond pixels) centered on the neutral line. Figures 2–4 show this area in 3 visible wavelengths and soft X-rays at 3 stages in the development of the event.

At 09:02, a small flare began in a region with emerging and cancelling flux, in the lower left corner of each panel in the figures (Fig. 2). At the same time (coincidence or trigger?), weak flare emission began to appear in H_α in the lower right in a purely monopolar area. This emission spread in area for the next 40 minutes (Figure 3), following a tortuous path upwards, toward the sunspot in the center. The spreading occured in the following way: a bright flash appeared at the base of each fibril or spicule in the path, followed by brightening then disappearance of the individual fibril, dissolving into a diffuse glow in the entire vicinity. This sequence can of course be interpreted in in terms of energy dumped suddenly in the low chromosphere at a footpoint, followed by heating and diffusion. Yohkoh did not go into flare mode until 09:37, and the hard x-rays were not detectable until 09:41. At about 09:45, very bright emission appeared in H_α and even the wings of Na D (upper photosphere). At 09:47:30 (Figure 4), the hard x-rays shot up an order of magnitude, peaking a minute later (Figure 5). This explosion in hard x-rays coincides with a rapid jump of optical emission to the pore on the right edge, just above center, of the field. At the same time there is a sharp increase in H_α emission in the far wings, which is seen in very small dots and arcs on the video images. At 09:49, the La Palma observer changed back to the large field of view to show the other set of flare footpoints (see Figure 6), just before Yohkoh sunset at 09:53. After this, the flare cooled gradually and very pretty H_α loops drained down into both ribbons (Figure 7).

Neither the H_α nor the magnetograms show any apparent cause for this flare: no flux cancellation and no sheared fibrils or neutral line. Both footpoints are in unipolar regions far from any polarity mixing and far from each other. So the instability must have been triggered high in the corona. Whatever caused the instability, the gradual buildup to it is recorded in the path across the photosphere of emission footpoints. We plan to measure the growth of the flare as total footpoint area vs. time throughout the buildup

and the impulsive phase. Since we have magnetograms accurately coaligned with the H_α emission maps, we can convert this curve from area to magnetic flux as a function of time. The derivative of this, in Mx per second, gives a direct measure of the excitation (reconnection?) rate of field lines in the corona, due to the instability which releases energy for the flare. Thus, the high resolution photospheric observations give us an estimate of a very fundamental coronal quantity. In addition, if we think of the excitation mechanism as moving continuously from one field line to another in a limited coronal volume, we have observed the mapping of that motion onto the photosphere. So we have also observed the very complicated (perhaps even discontinuous?) path of footpoints of field lines along a presumably simple continuous path high in the corona. This is relevant to current theories of chaotic or turbulent coronal magnetic fields.

Many small flares in our other movies show clear examples of reconfiguration of the H_α fibrils, whose magnetic footpoints are cancelling as opposite polarities collide. Viewing the movies, one is compelled to interpret these as reconnections of the magnetic field lines in the H_α chromosphere. The magnetic cancellation may be caused by new flux emergence in a neutral zone, as discussed above, or by systematic flows of swarms of "old" flux tubes in a mature region. For example, regions AR 7194 and 7205 each showed ongoing H_α fibril reconnections over periods of several days in mid-June 1992. Although these flares are not impressive in x-ray intensity, they are understandable in terms of their magnetic evolution and thus they can serve as prototypes for chromospheric reconnection events. One could select some of the clearest examples of reconnection and to measure such quantities as the average flux cancellation rate, the flux involved in a single H_α fibril event (if this can be meaningfully defined), the duration of an event, and speeds of the H_α fibrils. We have no idea at this time what the soft X-ray coronal manifestation of these prototype events will be.

5.0 Spicules, Ellerman Bombs, and Micro-Flares

We believe our digital movies are substantially better and certainly more accessible than any available in the past. Therefore, there is some hope to make progress in physical understanding of these classic problems in chromospheric dynamics.

Spicules on the disk (or "fine dark mottles") are seen in the wings of H_α between about 0.5 and 1.0 Å from line center. They show "noisy" Doppler shifts, with bursts appearing and disappearing on timescales of 30 seconds or less. Downflows predominate, but bursts of both sign appear in one place with rather different time profiles. They seem to rise out of the magnetic elements in network boundaries, but the precise relationship with flux tubes and granulation remains unclear. We have observed quiet network areas in very good seeing with a sequence designed to resolve the motions in spicules. Every 75 seconds, it takes photospheric continuum and magnetogram followed by 5 sets of 5 H_α images each, at line center and offsets of ± 0.5 and ± 0.7 Å. Initial viewing of these H_α Doppler and magnetic movies has suggested the following hypothesis, based on a few clear examples: an upward- moving spicule is launched when a small ring of magnetic field (perhaps in the lane surrounding a single granule) collapses inwards to a point. We plan to test this more systematically by viewing a large sample of events at high magnification, in collaboration with Y. Suematsu of the National Astronomical Observatory of Japan (NAOJ).

The cause of Ellerman bombs is another long-standing mystery. Every active region has these emission features seen in the far wings of H_α (not at all in the core), often just outside of a sunspot penumbra. They tend to recur in the same place, and their brightness varies gradually on timescales of tens of minutes. The movie sequence described above for the July 3 flare is ideal for studying them, and several others days of high quality are also available. Casual viewing of movies and isolated magnetograms reveals small bipoles at the locations of some bombs, suggesting the flux cancellation or reconnection models which have been published. The proximity to penumbra supports this idea, since nearly horizontal field lines are present in the low chromosphere and bends or kinks might reconnect into closed loops. Some but not all bombs are also bright in the core of Na D, and strong Doppler features may also be present. A competing hypothesis is that bombs are somehow related to siphon flows along field lines. We will make sets of vector magnetograms for one or more regions with many bombs to see if bipoles are always present. We will also measure velocities in the low chromosphere using Na D to search for a hydrodynamical origin.

At our highest resolution, it seems that every active region always shows tiny, bright, explosive events in H_α line center scattered haphazardly throughout. While this may be overstated somewhat, transients are extremely common, and a movie viewer often has real difficulty deciding whether a region is flaring or not. The exact same comments have been made (by Loren Acton, for example) about the SXT movies of active regions, and similar transients have been carefully studied in the UVSP data by the MSFC group. We plan to coalign a set of H-alpha, magnetic, and soft x-ray movies showing many microflares and determine the correspondence (if any) between the chromospheric and coronal transients. Are any generalizations possible about the magnetic environment in which they occur?

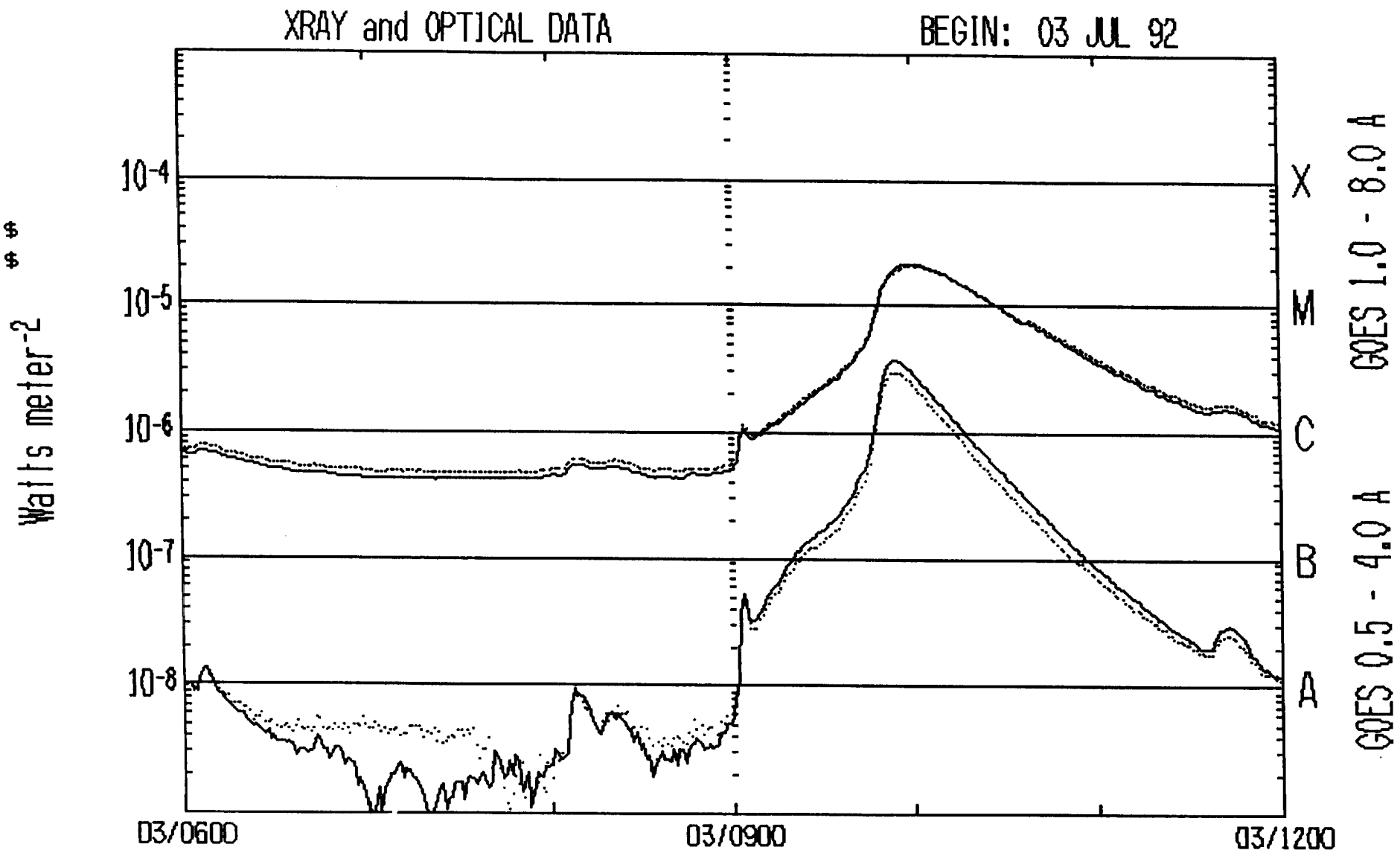

Figure 1. GOES Soft X-Ray Flux

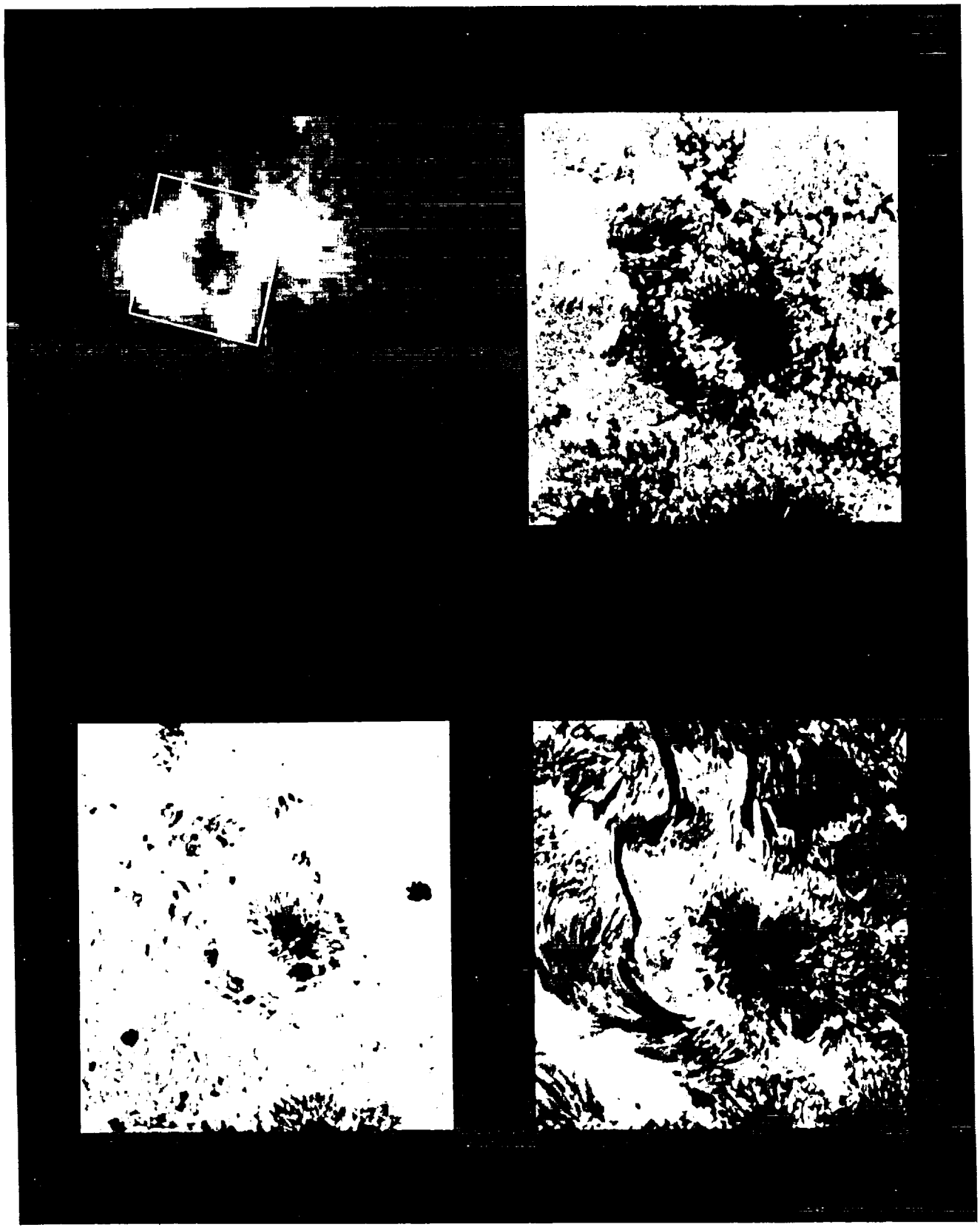

ORIGINAL PAGE
BLACK AND WHITE PHOTOGRAPH

Figure 2. Sample images at the time of the first small flare, around 9:03:40 on July 3, 1992. Clockwise from top left: Yohkoh/SXT image in soft X-rays, longitudinal magnetogram, H_α line center, and red continuum. Ground-based images have 112 arcsecond square field-of-view and 0.5 arcsecond resolution. The box on the SXT image shows the La Palma field-of-view.

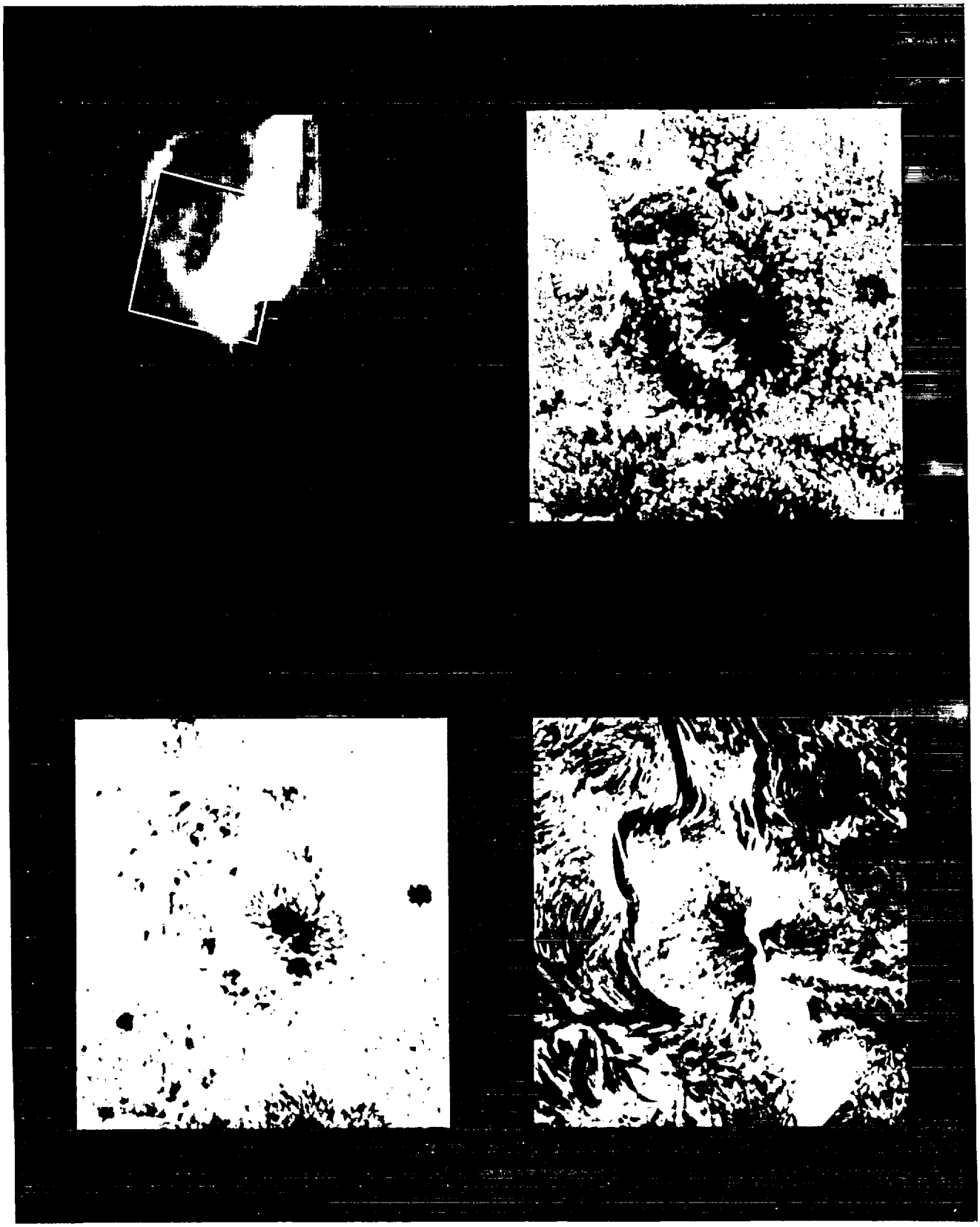

ORIGINAL PAGE
BLACK AND WHITE PHOTOGRAPH

Figure 3. Sample images in the gradual phase of the flare, around 9:43:03. One of the strands of the twisted filament, which runs vertically on the left side of the La Palma field, has just lit up (a micro-flare?). Same format as Fig. 2.

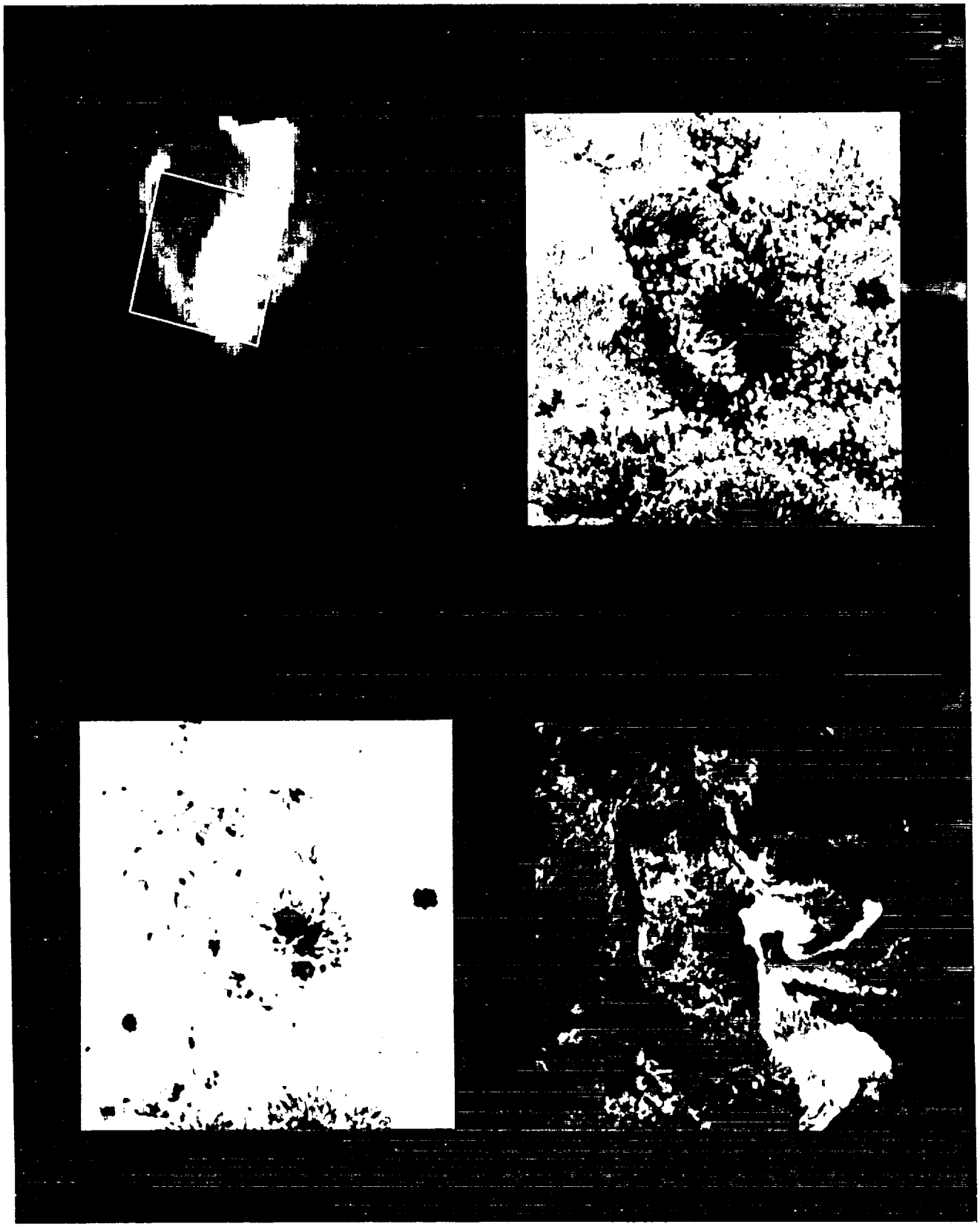

ORIGINAL PAGE
BLACK AND WHITE PHOTOGRAPH

Figure 4. The impulsive phase, around 9:48:33. Flare emission has just jumped to the pore on the right side. Same format as Fig. 2.

ORIGINAL PAGE
BLACK AND WHITE PHOTOGRAPH

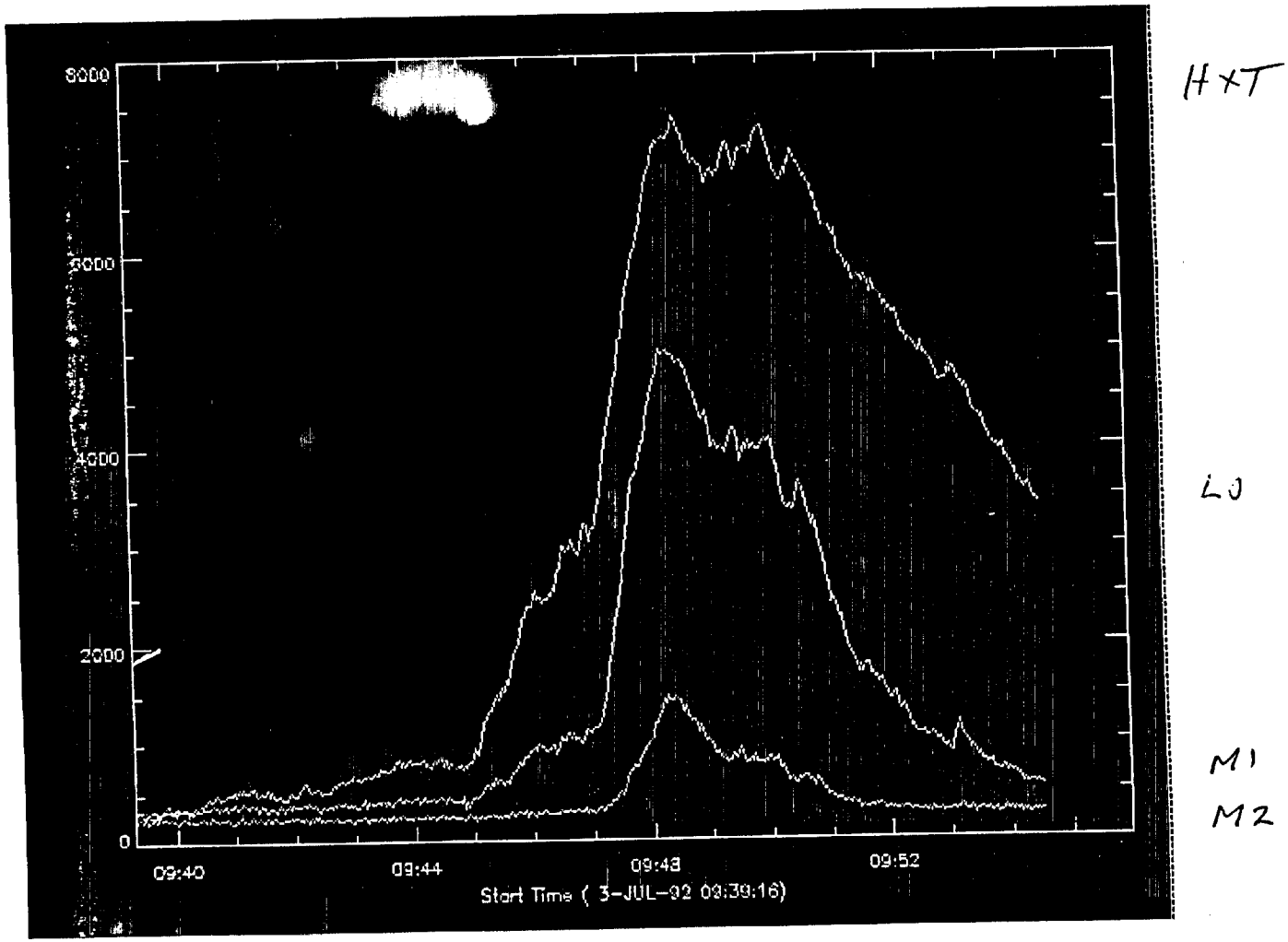

Figure 5. Hard X-ray fluxes in 3 energy bands, measure by the Yohkoh HXT.

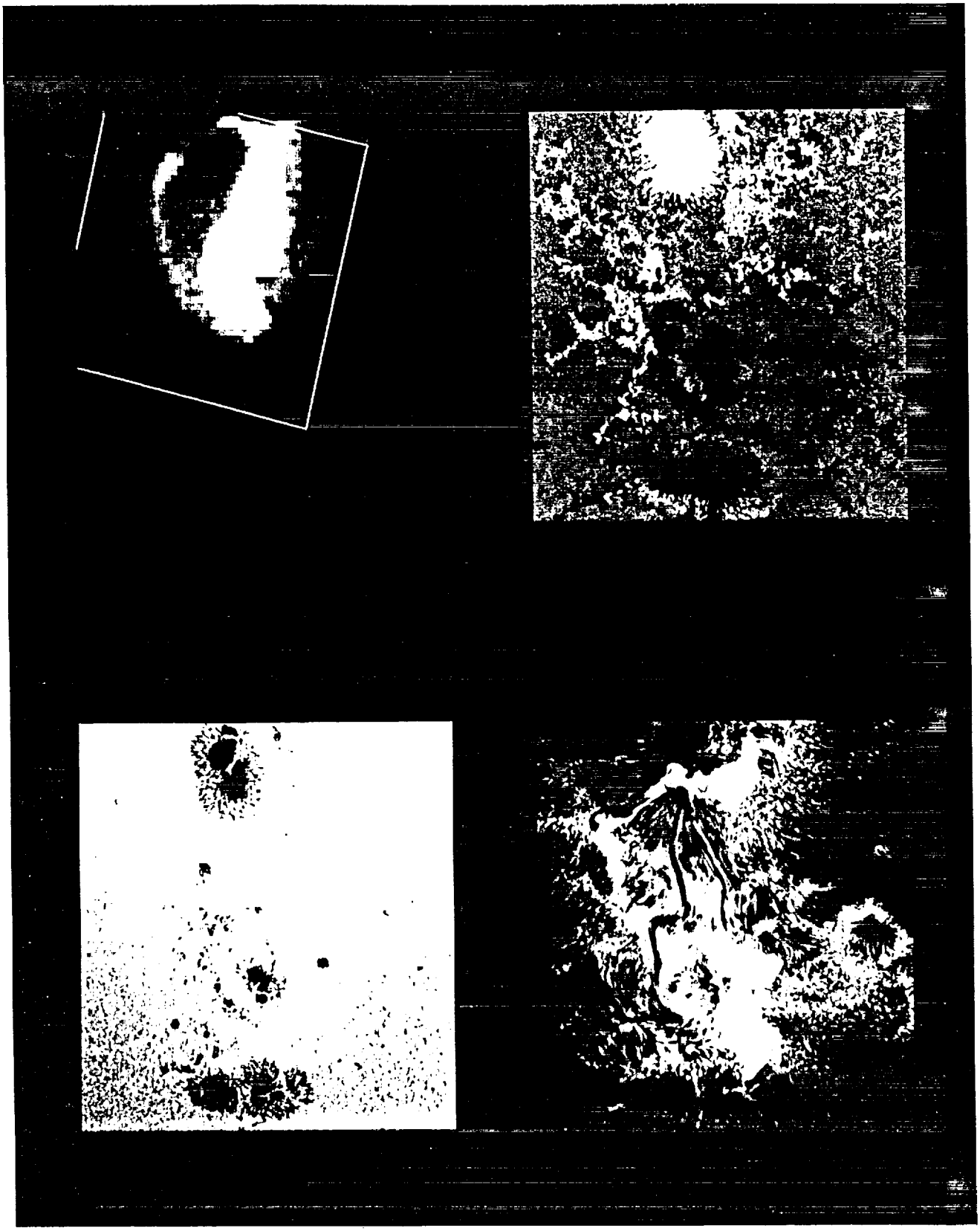

ORIGINAL PAGE
BLACK AND WHITE PHOTOGRAPH

Figure 6. Larger fields from La Palma (224 arcseconds square) just after the impulsive phase around 9:52:37, showing both flare ribbons.

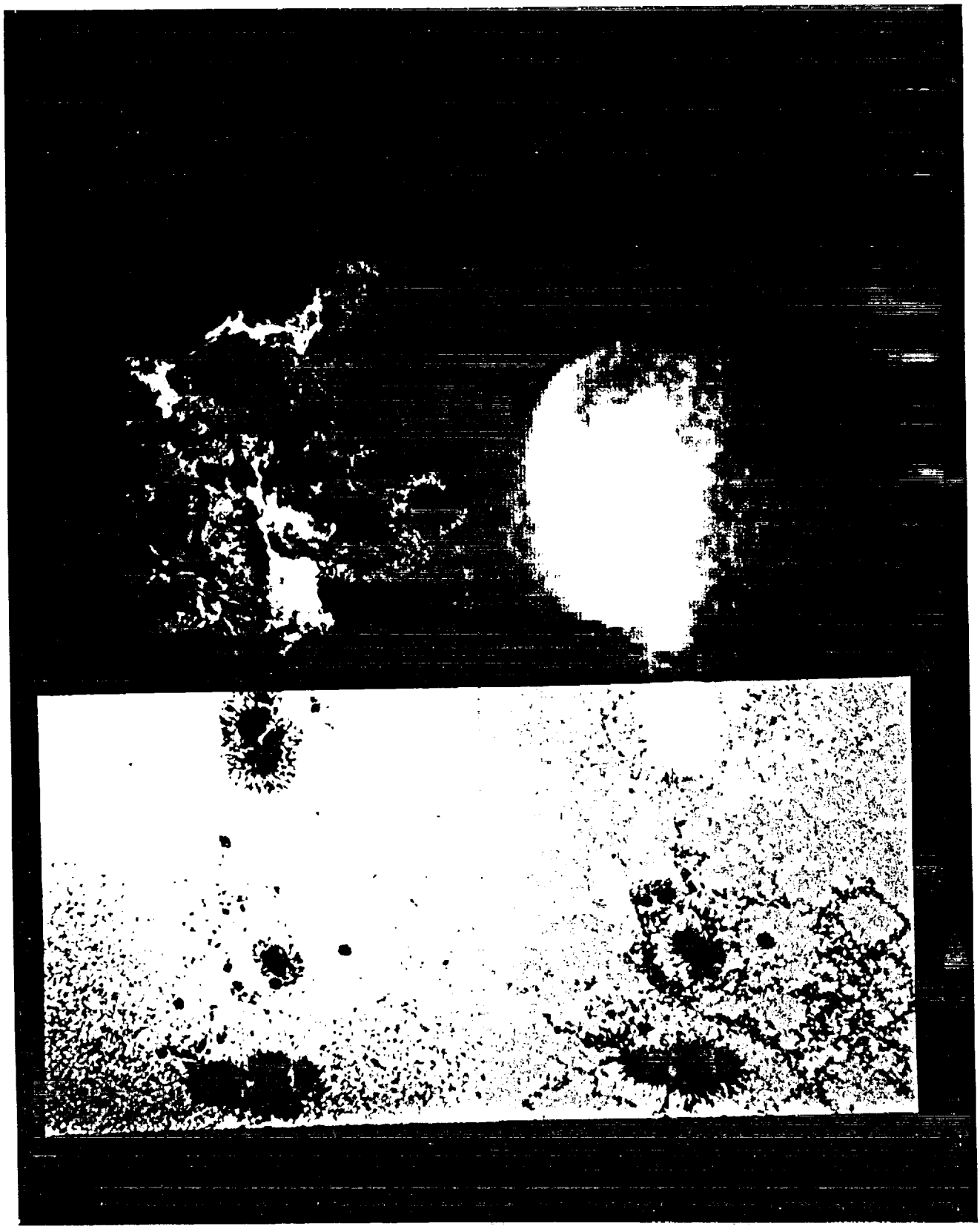

ORIGINAL PAGE
BLACK AND WHITE PHOTOGRAPH

Figure 7. Cooling phase around 10:45, showing crossed loops in H_α draining down into the footpoints.

Appendix D: Poster Paper from the AAS Meeting, January, 1993

Data Compression Experiments with High Resolution Solar Images

R. A. Shine (LPARL) and E. E. Majani (JPL)

Abstract

High resolution movies are a critical tool for solar physics but they generate enormous amounts of data. Data storage and transfers can be a major bottleneck for observations and analysis on the ground but it becomes especially acute for solar instruments on small spacecraft with limited telemetry and on board storage capabilities. Recently there has been a great deal of progress in data compression techniques, especially in the area of "lossy" techniques for continuous-tone images. These have the potential of reducing the storage and telemetry requirements of images by a factor of 10 or more while maintaining adequate quality for visual display. We have experimented with lossless and lossy techniques for a variety of photospheric, chromospheric, and coronal images. Algorithms used include the baseline JPEG (Joint Photographics Expert Group), the EPIC (Efficient Pyramid Image Coder), and the HCOMPRESS method. We indeed find that images and movies can reproduced from data compressed by factors from 10 to 20 which are virtually indistinguishable from the original to the eye. However, a visually acceptable image may not be adequate for more detailed analysis of solar movies, such as tracking structures, or the combination of images to form magnetograms or dopplergrams. Hence we have also experimented with analyzing data with different levels of compression to establish guidelines on the amount of compression tolerable for various types of analysis that might be performed on solar movies.

Methods

Three publicly available and well documented lossy methods were investigated but after preliminary experiments we concentrated on the JPEG algorithm for more detailed studies. The 3 techniques are:

1. baseline JPEG (Joint Photographics Expert Group) algorithm from the Independent JPEG Group, archive available on UUNET. This method is based on DCT's of 8×8 subimages. Compression is based on sorting, quantizing, and run-length/Huffman coding of the transform.

2. HCOMPRESS, from Richard White at the Space Telescope Science Institute. This data compression scheme is being used for the distribution of the digital sky survey (done for the guide star catalog for HST) to reduce it to a mere 100 CD-ROMs. It uses an H-transform of the entire image. This is a simple 2-D wavelet transform. As with the JPEG code, the transform is compressed by quantizing followed by lossless encoding of the approximate transform.

3. EPIC (Efficient Pyramid Image Coder) from the MIT Media Laboratory. This one is based on a biorthogonal wavelet (subband) decomposition and a combined run-length/Huffman entropy coder. It looks like it makes a tradeoff for a simple decoder

at the expense of a more complicated encoder – this is very reasonable for distributing images but the opposite of what one wants for spacecraft compression.

The documentation and sources for these were obtained via anonymous ftp and adapted for our image processing environments at both JPL and LPARL.

All of these methods store a transform of the image and lossy compression is accomplished by approximating the transform. Most of the compression comes from approximating the higher spatial frequencies (quantizing). They work well (i.e., good reproduction of the original with a high compression ratio) when the power is relatively low in the high frequency components. This is true of most continuous tone images and many solar images.

HCOMPRESS can be used in a lossless mode by not quantizing the transform. Similarly, JPEG and EPIC can be used in "almost" lossless mode (there is some loss from rounding to integers). If the high frequency amplitudes are low, this compression can be significant (factor of 4 or more for some solar images).

The amount of compression (and inversely, image quality) is easily controlled by the level of quantization applied.

Results

Initial experiments have been done with a variety of non-solar images using all 3 methods at JPL by one of us (Majani). Most of the work reported here on solar images has been done at LPARL.

Sample images shown are a x-ray coronal image from the SXT instrument on Yohkoh, a photospheric granulation image from Pic du Midi Observatory (digitized from film), and filtergrams taken with a CCD at the Swedish Solar Observatory (SSO) on La Palma. We have also experimented with other chromospheric and photospheric images (also taken at the SSO) with similar results.

SXT Coronal Image

Figure 1 shows an image from the SXT instrument on Yohkoh compared with a compressed version using JPEG. The original 8 bit image has an entropy of 6.67 bits/pixel and the first difference entropy is 4.69 bits/pixel. Our lossless compression code used 4.70 bits/pixel. This particular compressed image required an average of 0.75 bits per pixel, more than a factor of 10 less than the original. The two are essentially indistinguishable on the print and it is even difficult to find differences via blinking them on an image display. Table I shows the root mean square (rms) error for a range of JPEG compressions with increasing truncation of the DCT amplitudes. To demonstrate how and when the JPEG approximation starts to give an unsatisfactory approximation, we have a blowup of a portion of the image in figure 2 for a range of approximations. Starting with the $\times 8.4$ compression (corresponding to about 1 bit/pixel) some discrepancies can be seen in some of the faint small structures. (These images were printed with a low gamma to enhance the

fainter structures where most of the discrepancies are expected.) The problems increase with increasing compression but the $\times 20$ image is still hard to tell from the original when displayed normally. Much more of the high frequency information is lost in the $\times 53$ image and the 8×8 JPEG cell boundaries are obvious.

Photospheric Granulation

Figure 3 shows an image from a series taken at Pic du Midi which was digitized from film and then highly processed (this data set is described by Muller *et al.*, 1992, *Nature*, **356**, 322.). This particular data may be the best granulation movie to date and is representative of what could be obtained from a small solar telescope in space. Also in figure 3 are various levels of JPEG compression all of which are indistinguishable from the original in this print. Figure 4 shows a blowup of a subarea which reveals some differences. Very good quality is obtained with the 1.5 bits/pixel image but the 0.75 case is beginning to show some distortion of the smallest structures and some of the cell boundaries are beginning to become visible.

Figures 5 and 6 show results using the HCOMPRESS algorithm. It does not perform as well as JPEG for this images but this version of HCOMPRESS was "tuned" for photographic plates and a version better tuned for the noise characteristics of solar images may work better.

One concern with the JPEG compression scheme was that the 8×8 cells would affect local correlation tracking calculations used to study horizontal motions in the solar photosphere. For high compression ratios the cell boundaries are readily visible which could cause a sharp local peak in the cross correlation at zero lag that might mask or bias the actual offset. Numerical experiments with these Pic du Midi granulation images show that any effect is small. To further investigate any possible effects, we computed flow maps from a series of 100 of these granulation images with 3 levels of compression. The calculations were performed in the manner described in the Muller *et al.* paper. The results were quite good and the flow maps from all the compressions displayed in figure 3 gave compatible results. Comparing the average flow vectors for the original and the 1.5 bits/pixel compression showed an rms error in the velocity amplitudes of about 4% (or about 23 m/s out of the 564 m/s average velocity) with a bias in the distribution of only 0.4% (or 2 m/s).

Magnetograms

The computation of magnetograms and dopplergrams are more sensitive to errors since they depend on two or more filtergram images. A special concern for lossy representations was that ringing from the truncations of the high frequency components would cause artifacts in magnetograms which have regions of high contrast (where the polarity changes) and large areas of nearly zero signal.

Figure 7 shows a magnetogram computed from RCP and LCP filtergrams taken in the Fe 6302 line together with the same magnetogram computed from 3 different compressed versions of the data. These were done with a 12 bit JPEG code rather than the 8 bit version

used for the earlier examples. Each was constructed via our usual method of destretching the LCP image relative to the RCP image and then computing a line of sight magnetic signal from the difference of each pixel pair divided by the sum. The destretching was done after the compression and represents another step where compression errors could creep in.

From this example it seems that the filtergrams used to construct magnetograms can be compressed down to the 1.0 bit/pixel level without generating any distracting artifacts. Table II summarizes some of the errors in the compression of the original filtergrams and the rms errors in gauss for the (roughly) calibrated field strength. As would be expected, the largest errors are in the dark sunspot umbra where this method of measuring magnetic fields breaks down anyhow. The quality is surprisingly good and compressed filtergrams can certainly be used to construct magnetograms for most purposes. Some types of analysis, such as averaging a large number of magnetograms to improve signal to noise in a search for weak structures, are probably not feasible with compressed data.

Conclusions

Data compression techniques are now available that can provide an order of magnitude reduction in the storage and transmission requirements of solar images with sufficient accuracy for most scientific purposes. This study is not exhaustive but it shows that the JPEG scheme is already a feasible technique for spacecraft telemetry and data storage of coronal, chromospheric, and photospheric images. Improved data compression methods specialized for a particular class of solar images can probably be developed that perform somewhat better. The amount of compression can be varied to allow a tradeoff between compression and quality for different applications. In general we find that about 1 bit/pixel is sufficient to maintain data quality for most applications. Some coronal and chromospheric images can be compressed somewhat more (down to the 0.5 - 0.75 bit/pixel range) while well exposed photospheric images that will be used for constructing magnetograms or dopplergrams may need 1.5 bits/pixel. Effects from the JPEG cell boundaries and ringing from the high frequency approximations are surprisingly low for these compression levels. Some information is, of course, inevitably loss. In particular, accurate measurements of small faint structures will suffer. Also, it is probably not feasible to sum up a large number of compressed images to increase sensitivity – e.g., to look for very weak magnetic structures.

With the current emphasis on smaller scientific satellites with severe telemetry bottlenecks (e.g., a Gigabit or two per day for a SMEX), the feasibility of $\times 10$ data compression makes an enormous difference for solar imaging experiments.

Acknowledgements

Part of the research described in this abstract was performed at the Jet Propulsion Laboratory, California Institute of Technology, under contract with NASA. It was also supported by Lockheed Independent Research Funds and NASA contracts NAS8-39395 and NAS5-26813.

Figure 1. An SXT image from Yohkoh taken on 12-May-1992. The upper image is the original 8 bit image and the lower was reconstituted from a JPEG compressed file that used an average of 0.75 bits per pixel.

Figure 2. A portion of the SXT image in figure 1 showing the original and 5 levels of compression using JPEG.

Figure 3. A photospheric image of granulation and the image reconstructed from 3 different levels of JPEG compression. The bits/pixel required for each is indicated.

Figure 4. A blowup of part of the image shown in figure 3.

Figure 5. Same as figure 3 except that the HCOMPRESS algorithm was used. The bits/pixel required for each of the 3 compression levels is indicated.

Figure 6. A blowup of part of the image shown in figure 5.

Figure 7. Magnetograms constructed from right and left circularly polarized filtergrams in the Fe 6302 line for the original data and 3 different JPEG compressions as indicated.

Table I. Compression Statistics for SXT Image

bits/pixel	compression factor	rms error (counts)	rms/mean
4.59	1.7	0.57	0.008
2.84	2.8	1.91	0.028
1.73	4.6	2.89	0.042
1.21	6.6	3.39	0.049
0.95	8.4	3.68	0.054
0.77	10.	3.86	0.056
0.66	12.	3.99	0.058
0.50	16.	4.30	0.061
0.40	20.	4.36	0.064
0.31	26.	4.54	0.066
0.15	53.	5.16	0.075
0.08	95.	6.27	0.091

Table II. Compression Statistics for Magnetogram

bits/pixel	RCP rms/mean	LCP rms/mean	magnetogram rms (gauss)
2.92	.002	.002	13
2.06	.003	.003	18
1.25	.004	.004	28
0.85	.005	.005	35
0.52	.007	.007	48

Comparison of subareas from an SXT image with various JPEG compression factors. These are 100x100 pixel subareas of a region showing more structure than typical. The factors apply to the entire image.

fig 2

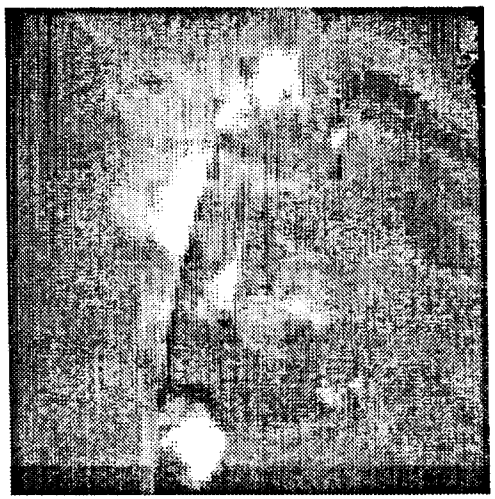

original

x 4.6

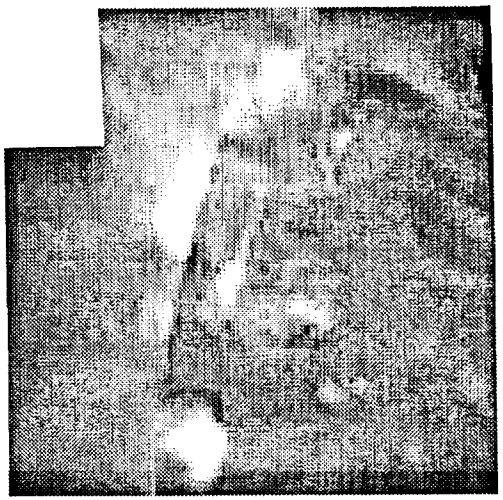

x 10.4

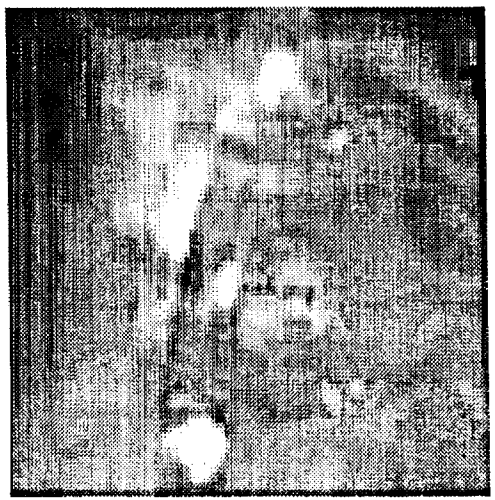

x 20

x 35

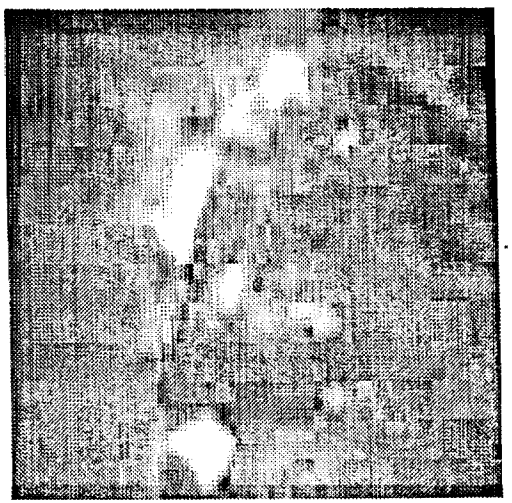

x 53

ORIGINAL PAGE
BLACK AND WHITE PHOTOGRAPH

512x512 pixel SXT image

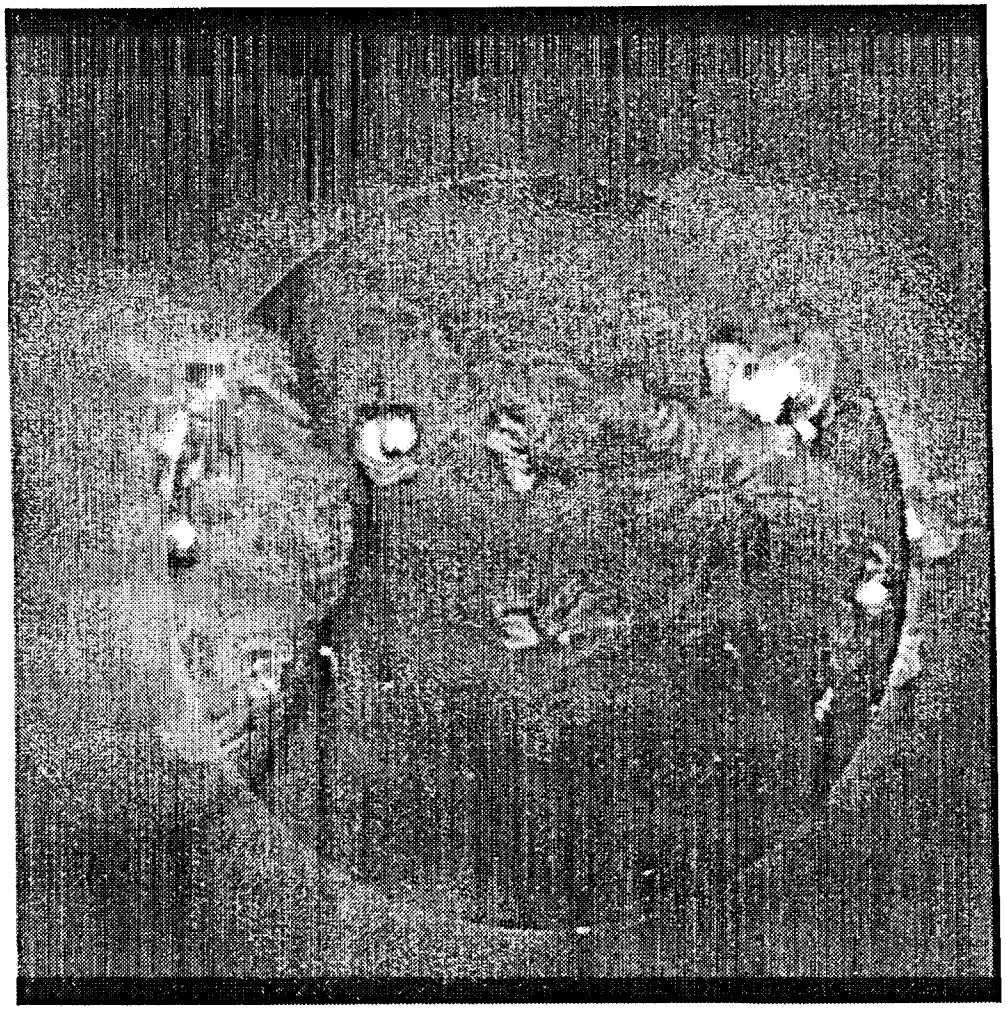

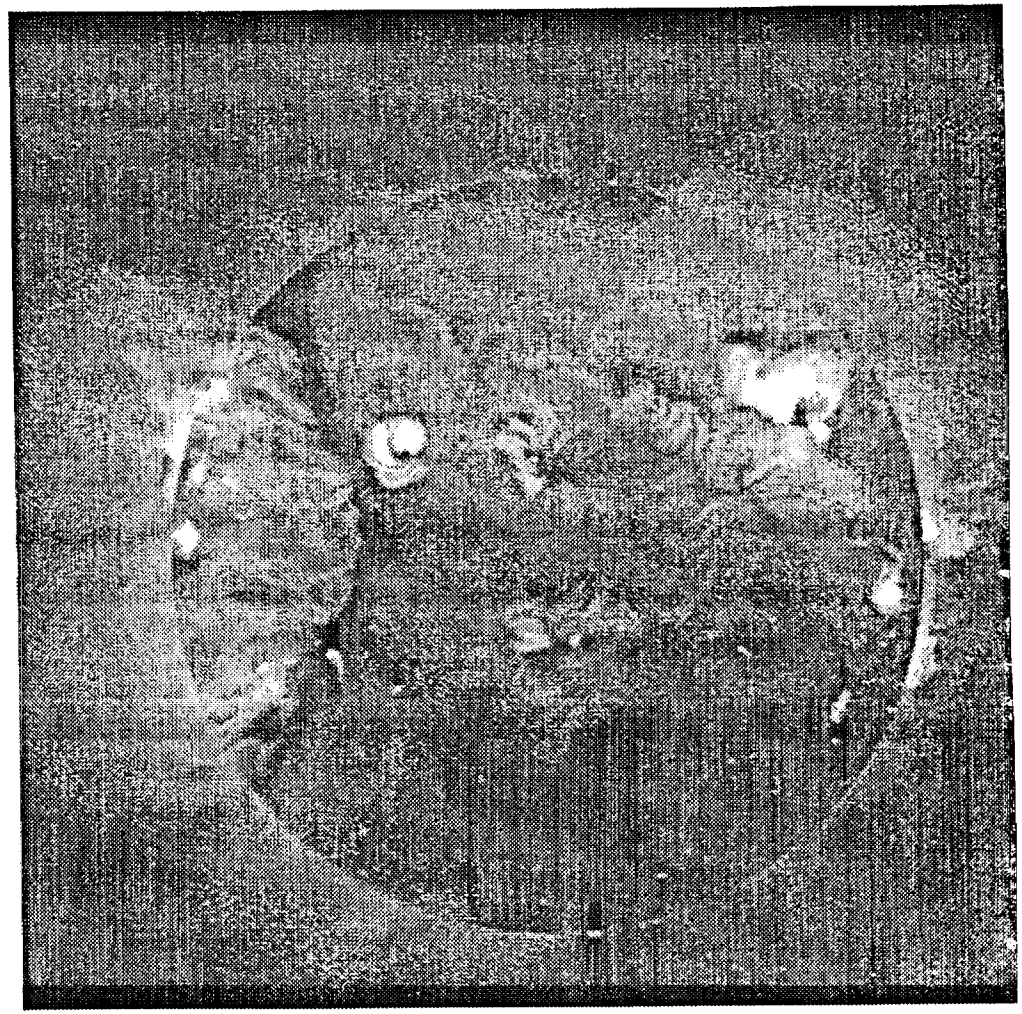

original

JPEG compressed x 10.4

Fig 1

ORIGINAL PAGE
BLACK AND WHITE PHOTOGRAPH

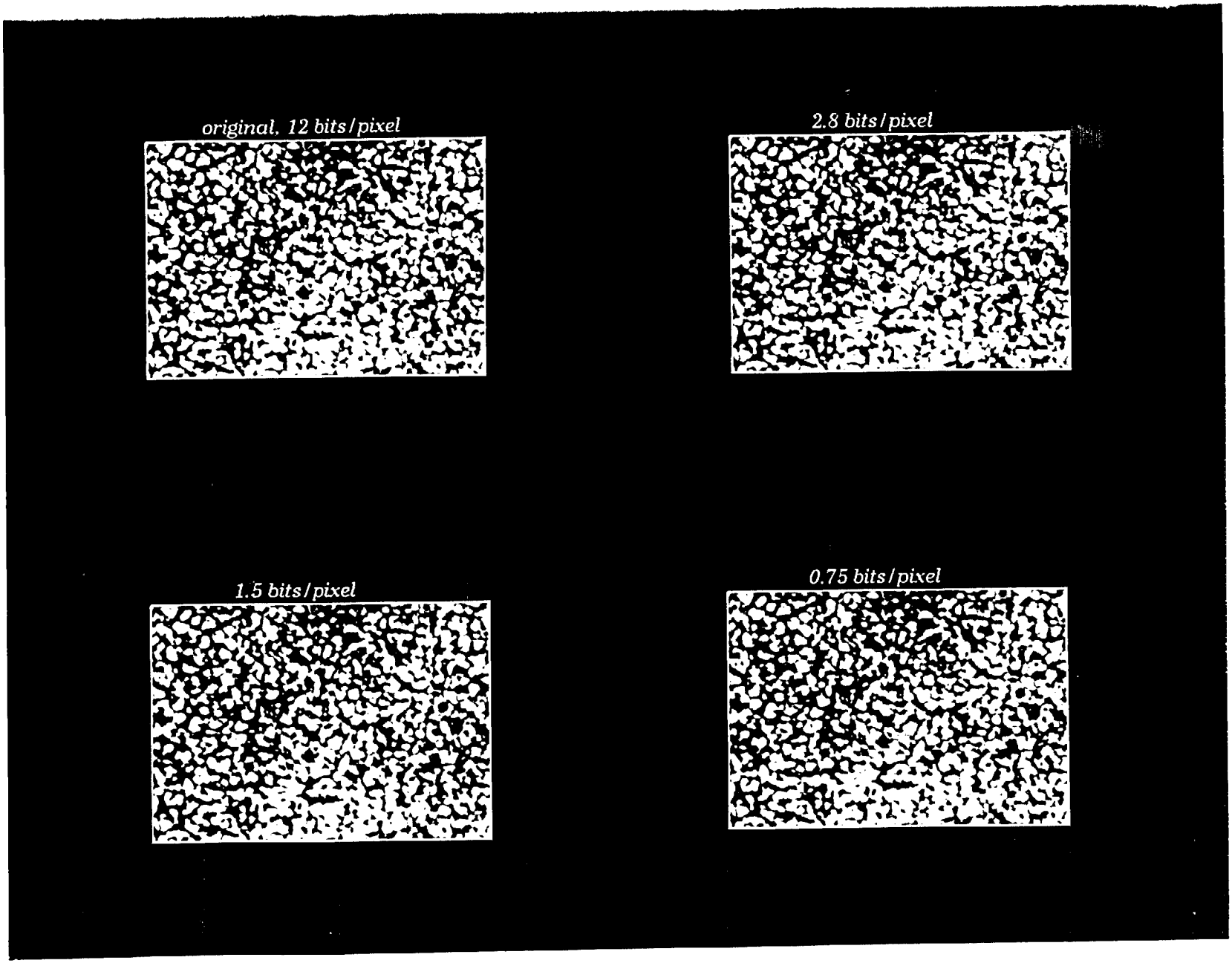

Figure 3. A photospheric image of granulation and the image reconstructed from 3 different levels of JPEG compression. The bits/pixel required for each is indicated.

ORIGINAL PAGE
BLACK AND WHITE PHOTOGRAPH
PRECEDING PAGE BLANK NOT FILMED

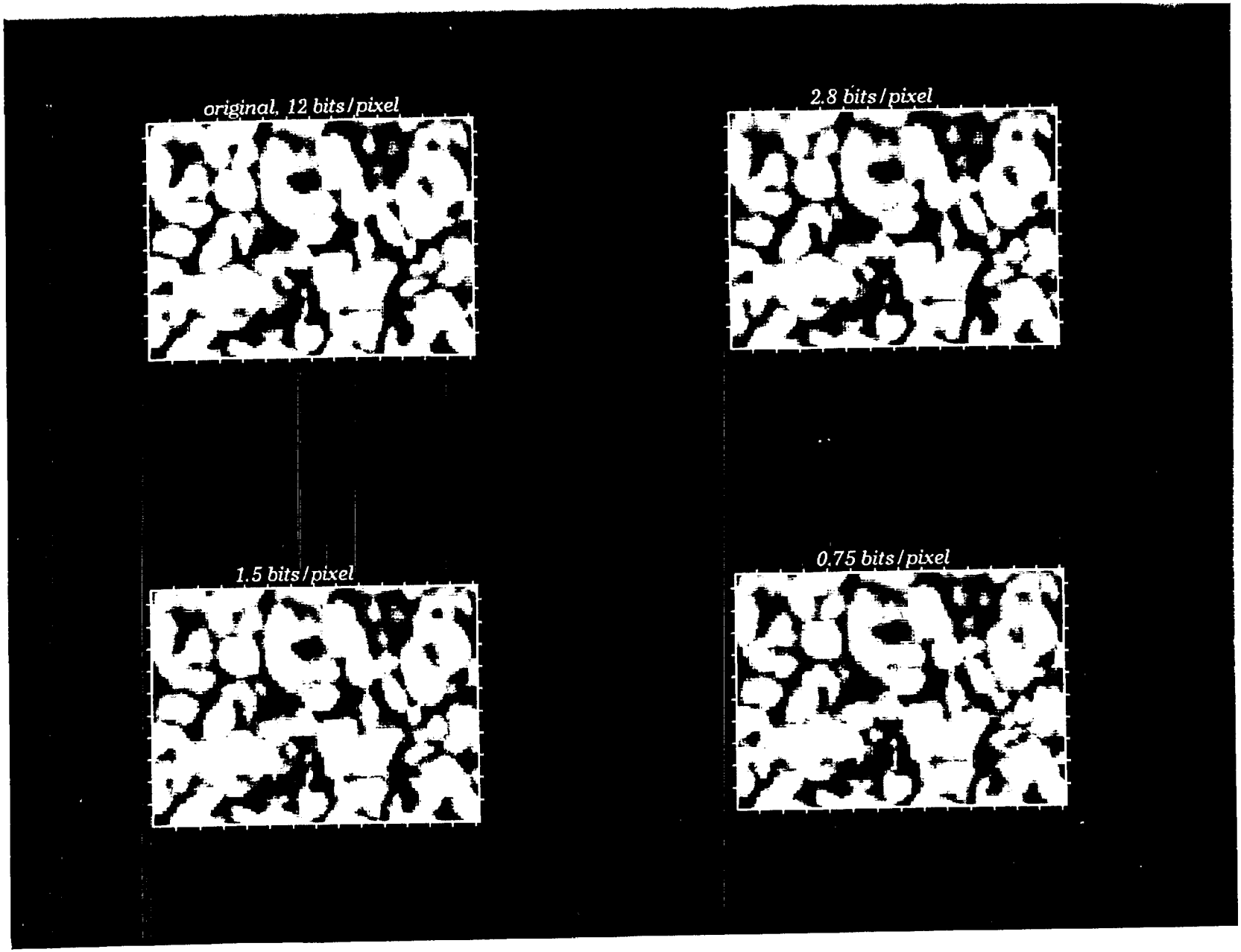

ORIGINAL PAGE
BLACK AND WHITE PHOTOGRAPH

Figure 4. A blowup of part of the image shown in figure 3.

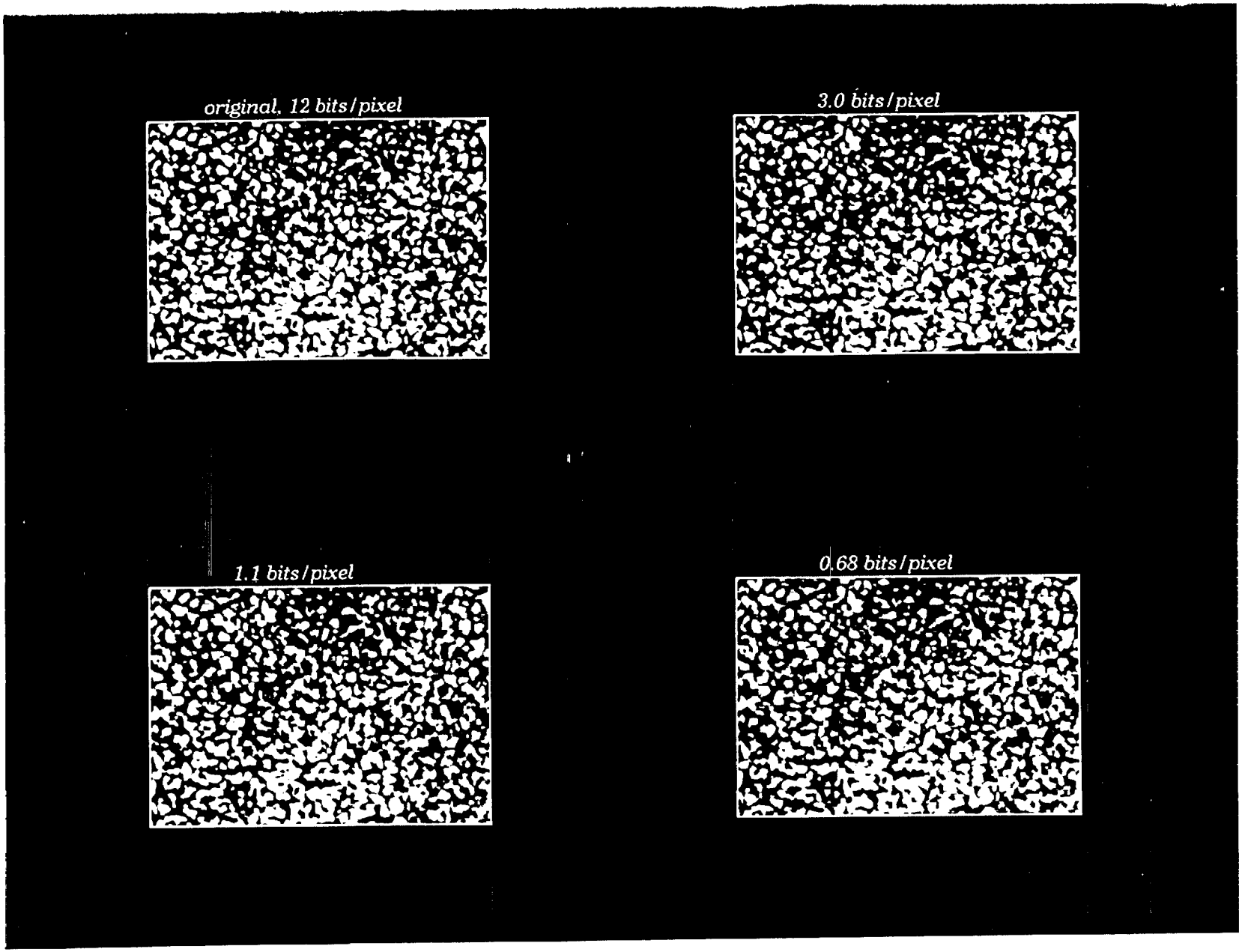

ORIGINAL PAGE
BLACK AND WHITE PHOTOGRAPH

Figure 5. Same as figure 3 except that the HCOMPRESS algorithm was used. The bits/pixel required for each of the 3 compression levels is indicated.

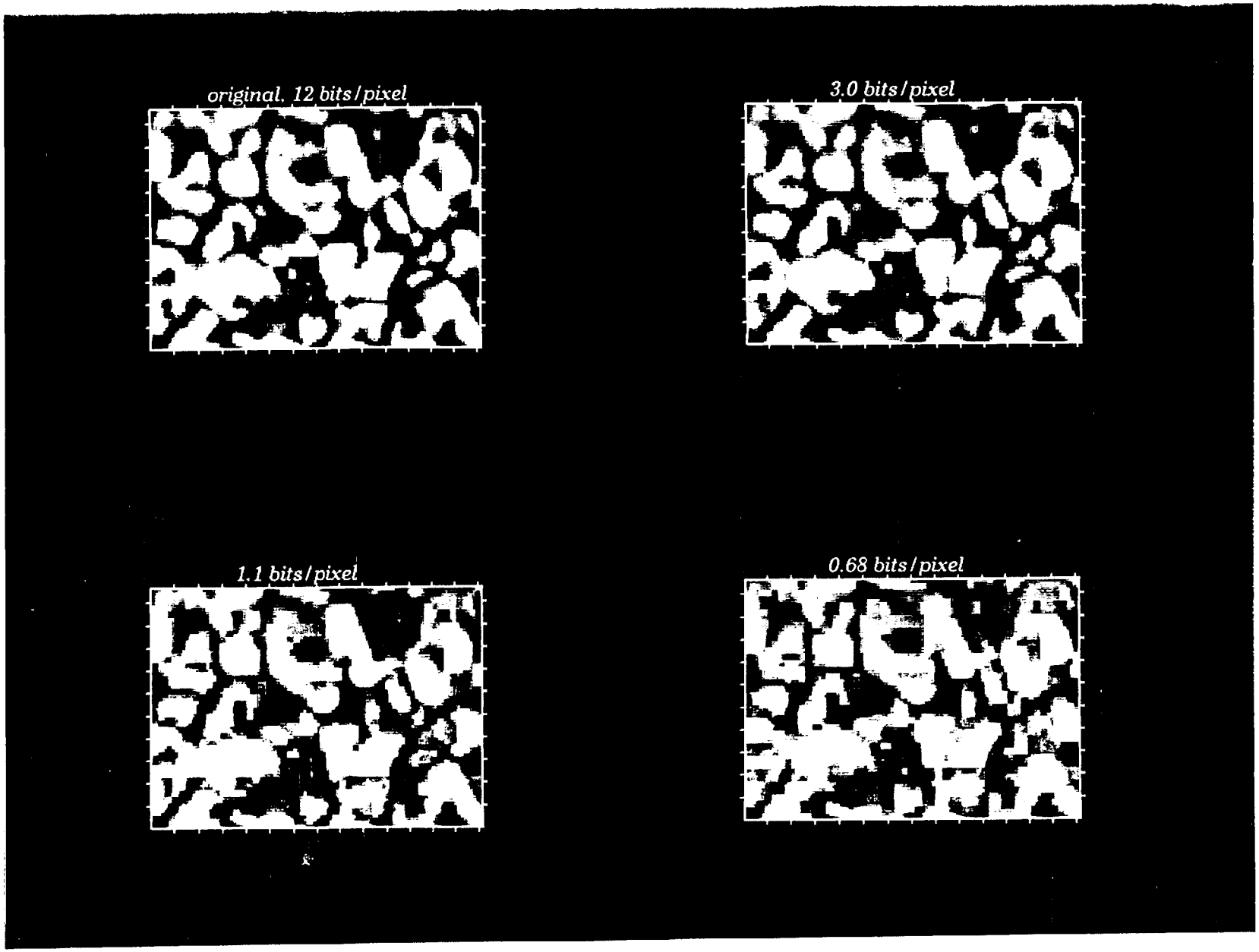

ORIGINAL PAGE
BLACK AND WHITE PHOTOGRAPH

Figure 6. A blowup of part of the image shown in figure 5.

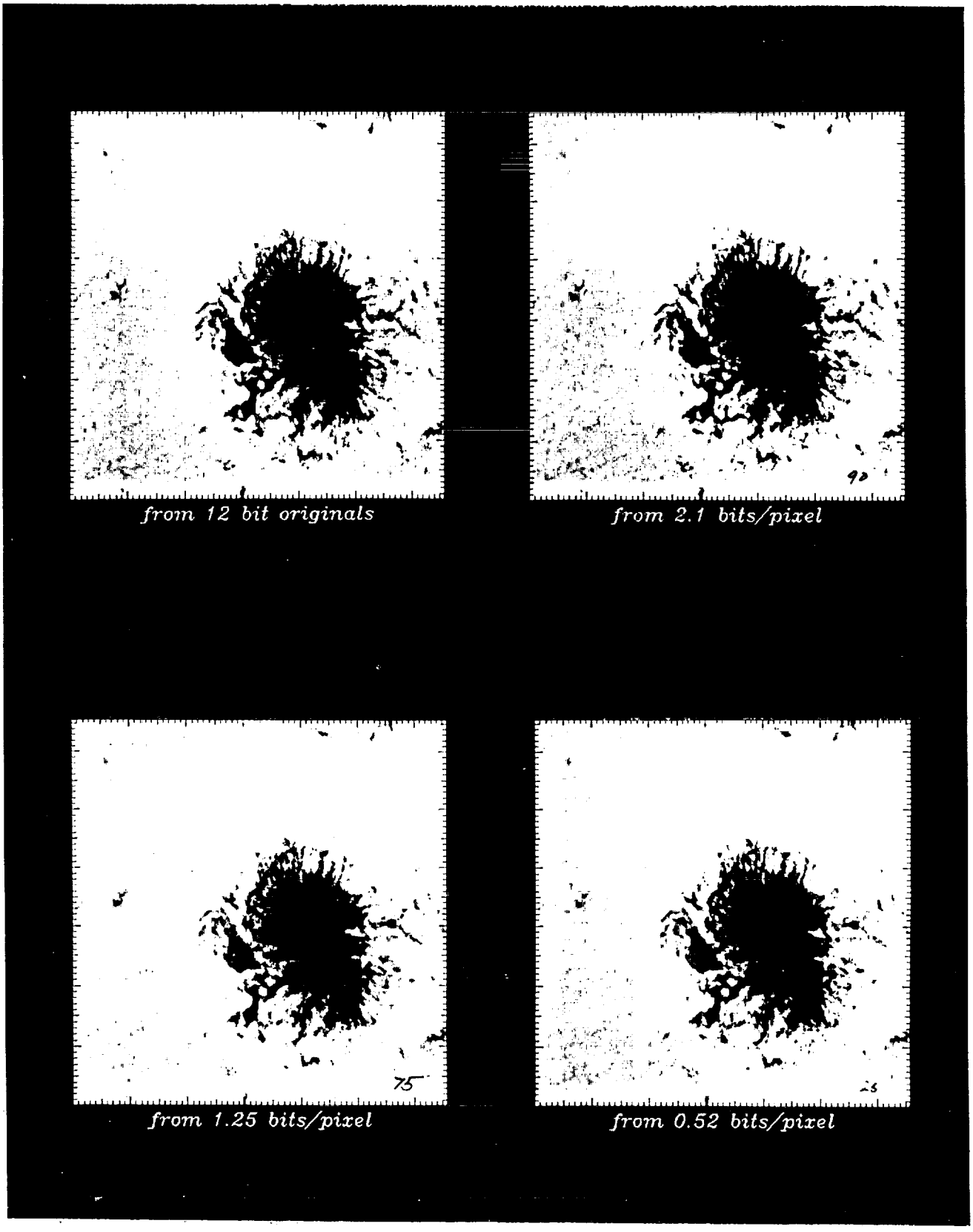

ORIGINAL PAGE
BLACK AND WHITE PHOTOGRAPH

gure 7. Magnetograms constructed from right and left circularly polarized filtergrams in the 6302 line for the original data and 3 different JPEG compressions as indicated.

NASA
National Aeronautics and Space Administration

Report Documentation Page

1. Report No.	2. Government Accession No.	3. Recipient's Catalog No.
LMSC/P073417		

4. Title and Subtitle

INVESTIGATION OF SOLAR ACTIVE REGIONS AT HIGH RESOLUTION BY BALLOON FLIGHTS OF THE SOLAR OPTICAL UNIVERSAL POLARIMETER, Extended Definition Phase.

5. Report Date

6. Performing Organization Code

7. Author(s)

Dr. Theodore D. Tarbell

8. Performing Organization Report No.

10. Work Unit No.

9. Performing Organization Name and Address

Lockheed Missiles and Space Co., Inc.
Lockheed Palo Alto Research Laboratory
3251 Hanover St., Dept. 91-30, B/252
Palo Alto, CA 94304

11. Contract or Grant No.

NAS8-39395

13. Type of Report and Period Covered

FINAL
May 1992 to May 1993

12. Sponsoring Agency Name and Address

National Aeronautics and Space Administration
George C. Marshall Space Flight Center
Marshall Space Flight Center, AL 35812

14. Sponsoring Agency Code

15. Supplementary Notes

16. Abstract

This contract supported technical studies of the feasability of balloon flights of the former Spacelab instrument, the Solar Optical Universal Polarimeter, with a modern charge-coupled device (CCD) camera, to study the structure and evolution of solar active regions at high resolution. In particular, different CCD cameras were used at ground-based solar observatories with the SOUP filter, to evaluate their performance and collect high resolution images. High resolution movies of the photosphere and chromosphere were successfully obtained using four different CCD cameras. Some of this data was collected in coordinated observations with the Yohkoh satellite during May-July, 1992, and they are being analyzed scientifically along with simultaneous X-ray observations.

17. Key Words (Suggested by Author(s))	18. Distribution Statement
CCD cameras, balloon flight, data compression, solar physics, solar magnetic fields, solar faculae.	Unclassified-Unlimited

19. Security Classif. (of this report)	20. Security Classif. (of this page)	21. No. of pages	22. Price
Unclassified	Unclassified	67	NSP

NASA FORM 1626 OCT 86